Cellular/Molecular

$Ca_v2.1$ in Cerebellar Purkinje Cells Regulates Competitive Excitatory Synaptic Wiring, Cell Survival, and Cerebellar Biochemical Compartmentalization

Taisuke Miyazaki,[1] Miwako Yamasaki,[1] Kouichi Hashimoto,[2,3,4] Maya Yamazaki,[5] Manabu Abe,[5] Hiroshi Usui,[6] Masanobu Kano,[3] Kenji Sakimura,[5,7] and Masahiko Watanabe[1,7]

[1]Department of Anatomy, Hokkaido University School of Medicine, Sapporo 060-8638, Japan, [2]Department of Neurophysiology, Graduate School of Biomedical Sciences, Hiroshima University, Hiroshima 734-8551, Japan, [3]Department of Neurophysiology, Graduate School of Medicine, The University of Tokyo, Tokyo 113-0033, Japan, [4]Precursory Research for Embryonic Science and Technology, Japan Science and Technology Agency, Saitama 332-0012, Japan, Departments of [5]Cellular Neurobiology and [6]Molecular Neuropathology, Brain Research Institute, Niigata University, Niigata 951-8585, Japan, and [7]Core Research for Evolutional Science and Technology, Japan Science and Technology Agency, Sanbancho, Chiyoda-ku, Tokyo 102-0075, Japan

In the adult cerebellum, each Purkinje cell (PC) is innervated by a single climbing fiber (CF) in proximal dendrites and 10^5-10^6 parallel fibers (PFs) in distal dendrites. This organized wiring is established postnatally through heterosynaptic competition between PFs and CFs and homosynaptic competition among multiple CFs. Using PC-specific $Ca_v2.1$ knock-out mice (PC-$Ca_v2.1$ KO mice), we have demonstrated recently that postsynaptic $Ca_v2.1$ plays a key role in the homosynaptic competition by promoting functional strengthening and dendritic translocation of single "winner" CFs. Here, we report that $Ca_v2.1$ in PCs, but not in granule cells, is also essential for the heterosynaptic competition. In PC-$Ca_v2.1$ KO mice, the extent of CF territory was limited to the soma and basal dendrites, whereas PF territory was expanded reciprocally. Consequently, the proximal somatodendritic domain of PCs displayed hyperspiny transformation and fell into chaotic innervation by multiple CFs and numerous PFs. PC-$Ca_v2.1$ KO mice also displayed patterned degeneration of PCs, which occurred preferentially in aldolase C/zebrin II-negative cerebellar compartments. Furthermore, the mutually complementary expression of phospholipase Cβ3 (PLCβ3) and PLCβ4 was altered such that their normally sharp boundary was blurred in the PCs of PC-$Ca_v2.1$ KO mice. This blurring was caused by an impaired posttranscriptional downregulation of PLCβ3 in PLCβ4-dominant PCs during the early postnatal period. A similar alteration was noted in the banded expression of the glutamate transporter EAAT4 in PC-$Ca_v2.1$ KO mice. Therefore, $Ca_v2.1$ in PCs is essential for competitive synaptic wiring, cell survival, and the establishment of precise boundaries and reciprocity of biochemical compartments in PCs.

Introduction

Cerebellar Purkinje cells (PCs) receive two excitatory afferents at distinct dendritic domains (Palay and Chan-Palay, 1974). In adulthood, single climbing fibers (CFs), which are projection fibers from the inferior olive, innervate the proximal dendrites of individual PCs, whereas distal dendrites or spiny branchlets are innervated by 10^5-10^6 parallel fibers (PFs) of cerebellar granule cells (GCs). This well-organized excitatory wiring is established through heterosynaptic competition between PFs and CFs and homosynaptic competition among multiple CFs in early postnatal development (Watanabe and Kano, 2011). In the first week of a rodent's life, multiple CFs innervate PC somata and form a dense plexus called the pericellular nest (Ramón y Cajal, 1911; Larramendi, 1969; Altman, 1972; Chedotal and Sotelo, 1992, 1993; Morara et al., 2001). Thereafter, single "winner" CFs translocate to PC dendrites, and the remaining perisomatic synapses formed by "winner" and "loser" CFs are subsequently eliminated, leading to the establishment of mono-innervation (Hashimoto et al., 2009). PF synaptogenesis and activity play an essential role in this refinement process (Woodward et al., 1974; Crepel et al., 1981; Mariani, 1982; Bravin et al., 1995; Sugihara et al., 2000).

This competitive excitatory wiring is regulated by various molecules expressed in presynaptic and postsynaptic elements of PC synapses, such as the metabotropic glutamate receptor mGluR1, P/Q-type Ca^{2+} channel, glutamate receptor GluRδ2 (GluD2), and precerebellin (or Cbln1) (Kano et al., 1995, 1997, 1998; Kashiwabuchi et al., 1995; Offermanns et al., 1997; Sugihara et al., 1999; Ichikawa et al., 2002; Miyazaki et al., 2004; Hirai et al., 2005). Of these, the P/Q-type Ca^{2+} channel is the major postsynaptic Ca^{2+} channel in PCs and mediates Ca^{2+} influx dur-

Received June 3, 2011; revised Nov. 20, 2011; accepted Nov. 23, 2011.

Author contributions: T.M., K.H., M.K., and M.W. designed research; T.M. and Mi.Y. performed research; K.H., Ma.Y., M.A., H.U., M.K., and K.S. contributed unpublished reagents/analytic tools; T.M. and Mi.Y. analyzed data; T.M., Mi.Y., and M.W. wrote the paper.

This research was supported by Grants-in-Aid for Scientific Research 19100005 (M.W.), Precursory Research for Embryonic Science and Technology (K.H.), and the Strategic Research Program for Brain Sciences (Development of Biomarker Candidates for Social Behavior; M.K.) from the Ministry of Education, Culture, Sports, Science, and Technology of Japan. We thank Dr. Yoshinobu Kawamura of Hiroshima University for technical advice and Rie Natsume of Niigata University for technical support.

Correspondence should be addressed to Masahiko Watanabe, Department of Anatomy, Hokkaido University School of Medicine, Sapporo 060-8638, Japan. E-mail: watamasa@med.hokudai.ac.jp.

DOI:10.1523/JNEUROSCI.2755-11.2012

 0270-6474/12/321311-18$15.00/0

ing strong depolarization elicited by CFs (Kano et al., 1992; Konnerth et al., 1992; Regehr and Mintz, 1994). In mice, global gene knock-out (KO) of the pore-forming subunit $Ca_v2.1$ (α1A) of P/Q-type Ca^{2+} channels causes regressed CF territory down to the soma and basal region of proximal dendrites and severe persistence of multiple CF innervation (Miyazaki et al., 2004). Furthermore, the loss of $Ca_v2.1$ function has profound effects on the pattern and territory of PF innervation and survival of PCs (Herrup and Wilczynski, 1982; Heckroth and Abbott, 1994; Rhyu et al., 1999a,b; Miyazaki et al., 2004; Sawada et al., 2009). Because the P/Q-type Ca^{2+} channel is also the major presynaptic Ca^{2+} channel involved in transmitter release (Mintz et al., 1992; Stea et al., 1994; Westenbroek et al., 1995), it is important to determine the synaptic and cellular locations in which P/Q-type Ca^{2+} channels perform these functions.

To answer this question, we have recently created a mouse model in which $Ca_v2.1$ is deleted in PCs (PC-$Ca_v2.1$ KO mice). Using this model, we demonstrated that postsynaptic $Ca_v2.1$ plays an essential role in homosynaptic competition, because functional strengthening and dendritic translocation of single winner CFs are severely impaired in PC-$Ca_v2.1$ KO mice (Hashimoto et al., 2011). In the present study, we report that $Ca_v2.1$ in PCs regulates heterosynaptic competition, cell survival, and the formation of precise boundaries and reciprocity of biochemical cerebellar compartments in PCs.

Materials and Methods

Animals. All animal experiments were performed according to the guidelines for the care and use of laboratory animals of the Hokkaido University School of Medicine. PC-$Ca_v2.1$ KO mice, in which $Ca_v2.1$ is deleted in PCs as early as postnatal day 2 (P2), were produced as described previously (Hashimoto et al., 2011). Briefly, $Ca_v2.1$-floxed mice ($Ca_v2.1^{lox/lox}$) were crossed with D2CreN mice ($GluD2^{Cre/+}$) to yield $Ca_v2.1^{lox/lox}$; $GluD2^{+/+}$ (control) mice and $Ca_v2.1^{lox/lox}$; $GluD2^{Cre/+}$ (PC-$Ca_v2.1$ KO) mice. For production of global Cav2.1 KO mice, $Ca_v2.1$-floxed mice were crossed with TLCN-Cre mice (Nakamura et al., 2001; Fuse et al., 2004) to yield heterozygous KO mice. Heterozygous mice were further interbred to generate homozygous KO mice and to eliminate the introduced Cre gene from the line. In the present study, we produced GC-specific Cav2.1 KO mice (GC-$Ca_v2.1$ KO mice) by crossing $Ca_v2.1$-floxed mice with E3CreN mice ($GluN2C^{iCre/+}$), in which the Cre gene was expressed in cerebellar GCs under the control of the GluN2C (GluRε3 or NR2C) promoter, as described below.

A C57BL/6 BAC genomic clone RP23–117K15, which contains the GluN2C gene (*Grin2c*), was purchased from the BACPAC Resources Center. The Quick and Easy BAC Modification Kit (Gene Bridges) was used for vector construction. We designed a gene-targeting vector in which the codon-improved Cre recombinase (iCre) gene was placed just behind the translation initiation site of the GluN2C gene in frame. Fragments of the iCre coding sequence and SV40 poly(A) were amplified by PCR from pBlue–iCre and pIRES–EGFP (Clontech), respectively, and ligated into pDTMC/FRTpgkgb2Neo (modified from pgkgb2Neo; Gene Bridges) containing a pgk/gb2–Neo cassette flanked by two *frt* sequences. This construct was used as the PCR template for the amplification of the fragment composed of the iCre–Neo cassette. By using two primers, Grin2cMet-iCre/sense (5′-TACC TCTCTCTGTGCCTGCTCTGATTTCTCTGCAGGACCCTCCAGTGGA CATGGTGCCCAAGAAGAAGAG-3′) and FRT3′/antisense (5′-GGTTGG TATTGTTGACCCCGATGGTGAGTGGCTGGATCTCCAGAGGCAAG GATATCGACTCACTATAGGGCTCGAG-3′), the cassette attached by 5′ and 3′ homology arms was amplified by PCR and then recombined into the translation initiation site of the GluN2C gene in RP23–117K15. The ~21.5 kb fragment containing the exon 1–11 of the GluN2C gene and the iCre–Neo cassette was subcloned into pDT–MC#3 vector (modified from pPauDT3; Yanagawa et al., 1999), including an MC1-promoter-driven diphtheria toxin gene. The resulting construct contained the translation initiation site of the GluN2C gene inserted by the iCre–Neo cassette, 8.1 kb upstream and 10.4 kb downstream genomic sequences, and 4.4 kb pDT–MC#3. To establish the E3CreN mouse line, we introduced the linearized targeting vector into the C57BL/6N-derived ES line RENKA and then selected recombinant clones under the medium containing 175 μg/ml G418. Culture of ES cells was performed as described previously (Mishina and Sakimura, 2007). The targeted clones were confirmed by Southern blot analysis using the SpeI-, EcoRI-, and EcoRV-digested genomic DNA hybridized with 5′, 3′, and iCre probes, respectively (see Fig. 5*B*). A 362 bp fragment of the genomic sequence was generated by PCR with the primers 5′-GTCTAGAGGTGAGT CTCGTG-3′ and 5′-GGCCTGTCTCAAAGCTGTG-3′ and used as the 5′ probe for Southern blot analysis. A 305 bp fragment was generated by PCR with the primers 5′-CCCTGGCTCATTGGAACTTG-3′ and 5′-TTTTCA CTGGGGTCTCATGG-3′ and used as the 3′ probe. A fragment of iCre coding sequence was obtained from pBlue–iCre and used as the iCre probe. Generation of chimeric mice was performed as described previously (Mishina and Sakimura, 2007). Briefly, targeted clones were microinjected into eight-cell-stage embryos of a CD-1 mouse strain. The resulting chimeric embryos were developed to the blastocyst stage by incubation for >24 h and then transferred to a pseudopregnant CD-1 mouse uterus. Germ-line chimeras were crossed with C57BL/6N female mice, and the heterozygous offspring were used as the E3CreN line. The heterozygous ($GluN2C^{iCre/+}$) and homozygous ($GluN2C^{iCre/iCre}$) mutant mice were viable, grew normally, and were fertile, as reported previously (Abe et al., 2004).

β-Galactosidase assay. To examine Cre recombinase activity in the brain of E3CreN mice, we crossed the E3CreN line with the Cre-inducible lacZ reporter mouse line (CAG-CAT-Z11) (Araki et al., 1995). The offspring carrying both the iCre and CAG-CAT-Z11 genes ($GluN2C^{iCre/+}$; *CAG-CAT-Z11*/+) were used as Cre activity reporter mice, and β-galactosidase expression was examined by X-gal staining as reported previously (Tsujita et al., 1999).

Sections. In each morphological analysis, we analyzed three control mice and three mutant mice. Under deep pentobarbital anesthesia (100 mg/kg body weight, i.p.), mice were fixed transcardially with 4% paraformaldehyde (PFA) in 0.1 M sodium phosphate buffer (PB), pH 7.2, for light microscopy or 4% PFA/0.1% glutaraldehyde (GLA) in PB for immunoelectron microscopy, and microslicer cerebellar sections (50 μm in thickness) were prepared (VT1000S; Leica) for histological, histochemical, and neuronal tracer analyses. Some sections were counterstained by 0.5 μM propidium iodide for 10 min. For electron microscopy, mice were fixed with 2% PFA/2% GLA in 0.1 M cacodylate buffer, pH 7.2, and microsliced sections (400 μm in thickness) were prepared. Sections were treated with 1% osmium tetroxide for 15 min, dehydrated, and embedded in Epon812.

Antibodies. We used affinity-purified primary antibodies raised against the following molecules (host species): mouse calbindin (goat; Nakagawa et al., 1998); rat vesicular glutamate transporters VGluT1 and VGluT2 (guinea pig; Miyazaki et al., 2003); mouse phospholipase Cβ3 (PLCβ3) (guinea pig; Nomura et al., 2007); mouse PLCβ4 (rabbit; Nakamura et al., 2004); and mouse plasmalemmal glutamate transporter EAAT4 (rabbit; Yamada et al., 1996). In the present study, we produced antibodies against 87–105 and 314–363 amino acid residues of mouse aldolase C (NCBI Reference Sequence NM_009657) in the rabbit and guinea pig and 361–400 amino acid residues of mouse $Ca_v2.1$ (GenBank accession number U76716) in the guinea pig. Procedures for making these affinity-purified antibodies have been reported previously (Fukaya et al., 2006). The specificity of the aldolase C antibody was confirmed by identical immunostaining patterns in the mouse brain with use of the two non-overlapping antibodies (data not shown). The lack of cross-reactivity to aldolases A and B was confirmed by immunoblot detection of a single protein band at 40 kDa in HEK293 lysates transfected with the pTracer–CMV2 mammalian expression plasmid vector (Invitrogen) encoding aldolase C but not aldolase A or B (data not shown). The specificity of $Ca_v2.1$ antibody was confirmed by blank immunohistochemistry in global $Ca_v2.1$ KO mice and by selective loss of immunohistochemical signals in PF terminals in GC-$Ca_v2.1$ KO mice (see Fig. 5*E–N*).

Immunohistochemistry. Immunohistochemical incubations were done at room temperature using PBS, pH 7.2, containing 0.1% Triton X-100 (TPBS) for diluent and washing buffers. For immunofluorescence, most sections were successively incubated in a free-floating state with 10%

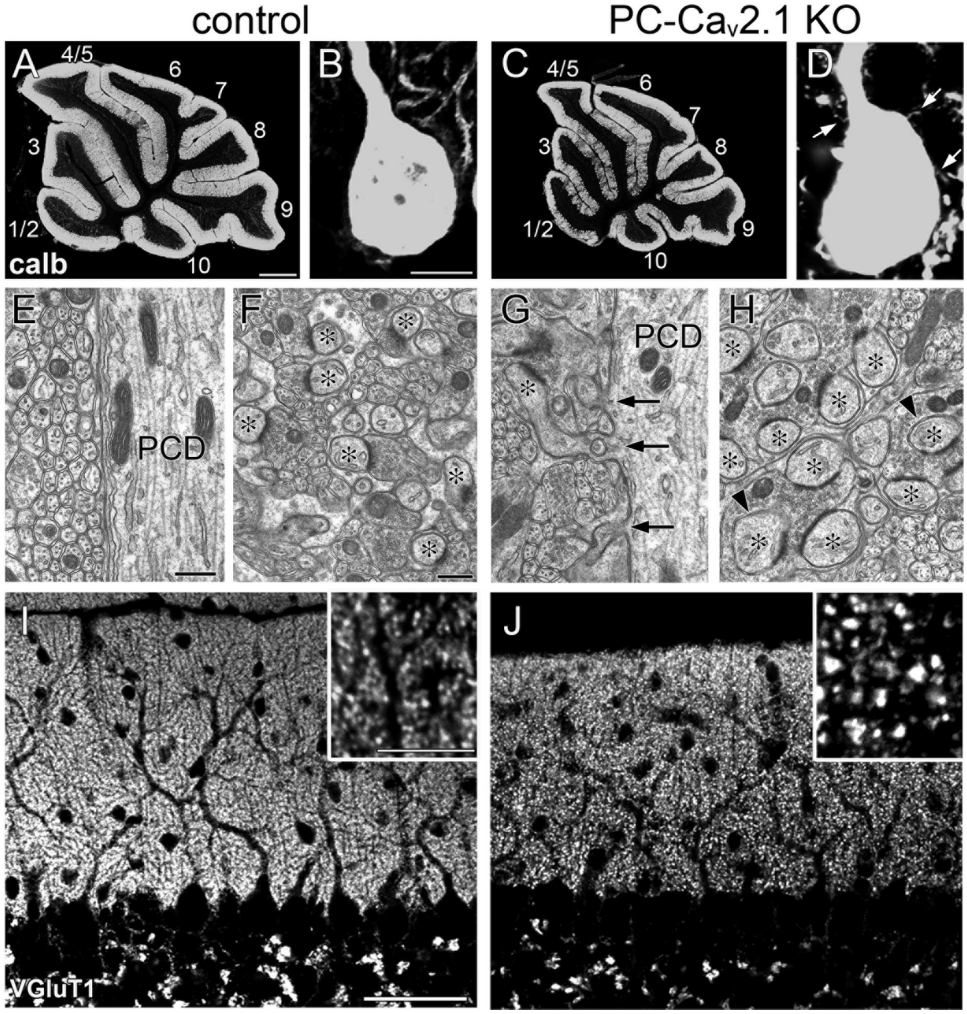

Figure 1. Enlargement of PF terminals and proximal expansion of PF territory in PC-$Ca_v2.1$ KO mice. ***A–D***, Immunofluorescence for calbindin (calb) in control (***A***, ***B***) and PC-$Ca_v2.1$ KO mice (***C***, ***D***). Arrows in ***D*** indicate spine-like protrusions from PC soma. The lobule number is indicated by numerals 1–10. ***E–H***, Electron micrographs showing shaft dendrites of PCs (PCD; ***E***, ***G***) and neuropil regions (***F***, ***H***) in control (***E***, ***F***) and PC-$Ca_v2.1$ KO (***G***, ***H***) mice. Arrows in ***G*** indicate ectopic spines from shaft dendrites. Asterisks in ***F*** and ***H*** indicate PC spines in contact with putative PF terminals. Arrowheads indicate PC spines thoroughly surrounded by enlarged PF terminals. ***I***, ***J***, Immunofluorescence for VGluT1 in control (***I***) and PC-$Ca_v2.1$ KO (***J***) mice. Scale bars: ***A***, 500 μm; ***B***, inset in ***I***, 10 μm; ***E***, ***F***, 500 nm; ***I***, 50 μm.

normal donkey serum for 30 min, a mixture of primary antibodies overnight (1 μg/ml), and a mixture of Alexa Fluor-488-, indocarbocyanine (Cy3)-, and indodicarbocyanine (Cy5)-labeled species-specific secondary antibodies (1:200; Invitrogen; Jackson ImmunoResearch) for 2 h or with 10 μM propidium iodide for 10 min (Invitrogen). For $Ca_v2.1$, we used fresh frozen sections mounted on silane-coated slide glasses, which were fixed with 4% PFA for 10 min and then subjected to immunofluorescence incubation as above. Images were taken with a laser scanning microscope (FV1000; Olympus) equipped with a helium–neon/argon laser and a PlanApo (10×/0.40) and a PlanApoN (60×/1.42, oil immersion) objective lens (Olympus). To avoid crosstalk between multiple fluorophores, Alexa Fluor-488 (or FITC), Cy3, and Cy5 fluorescent signals were acquired sequentially using the 488, 543, and 633 nm excitation laser lines. Single optical sections were obtained (640 × 640 pixels; pixel size, 110 nm).

To examine the change in parasagittal cerebellar compartments, we performed immunofluorescence for PLCβ3, PLCβ4, EAAT4, and aldolase C using horizontal cerebellar sections. Using MetaMorph software (Molecular Devices), the intensity of immunofluorescent signals was measured to obtain the gray density in the molecular layer of immunopositive (or strong) and immunonegative (or weak) compartments, from which we calculated the relative intensity gap between adjacent $P1^+$ and $P1^-$, $P2^+$ and $P2^-$, $P3^+$ and $P3^-$ regions, respectively (percentage; see Figs. 11*I*,*J*, 13*F*). We also measured the width of cerebellar compartments $P1^+$, $P1^-$, $P2^+$, $P2^-$, and $P3^+$ in lobules 3–6 (see Figs. 10*E*, 13*E*).

Immunoelectron microscopy. For preembedding immunogold electron microscopy, microslicer sections were incubated with 0.1% sodium borohydride in TPBS for 10 min. After incubation with blocking solution (Aurion) for 30 min, sections were incubated overnight with the primary antibody diluted with PBS containing 1% bovine serum albumin and 0.004% saponin and incubated with 1.4 nm gold-conjugated secondary antibody (1:200; Nanogold; Nanoprobes) for 3 h. After intensive washing in 0.004% saponin/PBS, sections were treated with 2% GLA in PB for 60 min and incubated with silver enhancement solution (SE-EM; Aurion) for 90 min. Sections were treated with 1% osmium tetroxide for 15 min, dehydrated, and embedded in Epon812.

Anterograde tracer labeling. Under anesthesia with chloral hydrate (350 mg/kg body weight, i.p.), a glass pipette (G-1.2; Narishige) filled with 2–3 μl of 10% solution of dextran Alexa Fluor-594 (DA-594; Invitrogen) in PBS was inserted stereotaxically into the inferior olive by the dorsal approach, as described previously (Miyazaki and Watanabe, 2011). Tracers were injected by air pressure (Pneumatic Picopump; World Precision Instruments). After 4 d, mice were anesthetized and fixed by transcardial perfusion. For combined labeling by tracer and immunofluorescence, DA-594-labeled microslicer sections were incubated with a mixture of calbindin and VGluT2 antibodies followed by incubation with fluores-

cent secondary antibodies for 2 h. Images of double or triple labeling were taken with a confocal laser-scanning microscope.

Fluorescent in situ *hybridization.* cDNA fragments of mouse PLCβ3 (nucleotide residues 2881–3812; GenBank accession number BC035928) and mouse PLCβ4 (nucleotide residues 230–1082; GenBank accession number AF332072) were subcloned into the Bluescript II plasmid vector. Digoxigenin- or fluorescein-labeled cRNA probes were prepared by *in vitro* transcription, as described previously (Yamasaki et al., 2001, 2010).

After anesthesia with diethyl ether, fresh brains were removed from the skulls and immediately frozen in powdered dry ice. Sections were treated with the following incubation steps: fixation with 4% PFA–PB, pH 7.2, for 10 min; washing in PBS for 10 min; acetylation with 0.25% acetic anhydride in 0.1 M triethanolamine-HCl, pH 8.0, for 10 min; and prehybridization for 1 h in a hybridization buffer (50% formamide, 50 mM Tris-HCl, pH 7.5, 0.02% Ficoll, 0.02% polyvinylpyrrolidone, 0.02% bovine serum albumin, 0.6 M NaCl, 200 μg/ml tRNA, 1 mM EDTA, and 10% dextran sulfate). Hybridization was performed at 63.5°C for 12 h in the hybridization buffer supplemented with cRNA probes at a dilution of 1:1000. Posthybridization washing was done at 61°C successively with 5× SSC for 30 min, 4× SSC containing 50% formamide for 40 min, 2× SSC containing 50% formamide for 40 min, and 0.1× SSC for 30 min. Sections were immersed at room temperature in NTE buffer (0.5 M NaCl, 0.01 M Tris-HCl, pH 7.5, and 5 mM EDTA), 20 mM iodoacetamide in NTE buffer, and in TNT buffer (0.1 M Tris-HCl, pH 7.5, and 0.15 M NaCl) for 20 min each. Immunohistochemical detection of hybridized probes was done using FITC–TSA and Cy3–TSA plus tryamide signal amplification kits (PerkinElmer Life and Analytical Sciences), as reported previously (Yamasaki et al., 2010).

Electrophysiology. Coronal slices (250 μm in thickness) were prepared from control and PC-$Ca_v2.1$ KO mice at P14–P21 as described previously (Hashimoto and Kano, 2003). Whole-cell recordings were made from visually identified PCs using an upright microscope (BX51WI; Olympus) at 31°C. Resistances of patch pipettes were 3–4 MΩ when filled with an intracellular solution composed of the following (in mM): 60 CsCl, 10 Cs D-gluconate, 20 tetraethylammonium-Cl, 20 BAPTA, 4 $MgCl_2$, 4 ATP, 0.4 GTP, and 30 HEPES, pH 7.3, adjusted with CsOH. The pipette access resistance was compensated by 80%. The composition of the standard bathing solution was as follows (in mM): 125 NaCl, 2.5 KCl, 2 $CaCl_2$, 1 $MgSO_4$, 1.25 NaH_2PO_4, 26 $NaHCO_3$, and 20 glucose (bubbled with 95% O_2 and 5% CO_2). Bicuculline (10 μM) was always added to block inhibitory synaptic transmission. Ionic currents were recorded with a patch-clamp amplifier (EPC10; HEKA). Glass pipettes of the same type as the recording electrodes were used for focal stimulation. Stimulation pipettes were filled with the standard saline and placed halfway between the PC layer and the pia mater at a position >200 μm lateral to the recorded PC to stimulate PFs. The stimulus consisted of balanced bipolar pulse pairs (100 μs anodal pulse, 100 μs gap, and 100 μs cathodal pulse) produced by a biphasic isolator (BAK Electronics), and selective stimulation of PFs was confirmed by paired-pulse facilitation of EPSCs with a 50 ms stimulation interval (Konnerth et al., 1990). For a minimal stimulation experiment, the stimulus intensity was gradually increased until a small all-or-none response was detected in PCs with a 40–50% failure rate. PCs were voltage clamped at −80 mV to record PF-mediated EPSCs (PF-EPSCs). The signals were filtered at 2 kHz and digitized at 20 kHz. Online data acquisition and offline data analysis were performed using PULSE software (HEKA). The decay time constant of PF-EPSCs was measured by fitting the EPSC decay with single exponential.

Results

In the present study, we investigated the cerebellum of PC-$Ca_v2.1$ KO mice to determine the role of PC-$Ca_v2.1$ in the cytological and synaptic development of PCs. For comparison, we also produced and examined the cerebellum of GC-$Ca_v2.1$ KO mice.

Expanded PF territory and enlarged PF terminals forming multiple contacts

Cerebellar histology and PC morphology were examined at P21 by immunofluorescence for calbindin, a marker of PCs in the cerebellum. In PC-$Ca_v2.1$ KO mice, the cerebellum was smaller in size than the cerebellum in control littermates, but its histology was grossly normal in terms of the foliation and laminar organization in the cerebellum (Fig. 1*A*,*C*) and the monolayer alignment and dendritic branching in PCs (see Fig. 4*A*,*D*). The reduced cerebellar size and normal dendritic branching are consistent with another line of PC-specific $Ca_v2.1$ KO mice, *Cacna1a*$^{purk(-/-)}$ (Mark et al., 2011; Todorov et al., 2011) and global $Ca_v2.1$ KO mice (Miyazaki et al., 2004). The surface of the somata and proximal dendrites was smooth in control mice (Fig. 1*B*) but considerably rough in PC-$Ca_v2.1$ KO mice (Fig. 1*D*, arrows). Electron microscopy revealed that the rough cell surface reflected frequent protrusion of spines or spine-like processes, and they formed asymmetrical synapses with nerve terminals (Fig. 1*E*,*G*). The number of spines per 1 μm of shaft dendrites (>2 μm in caliber) was significantly increased in PC-$Ca_v2.1$ KO mice (0.26 ± 0.05) compared with control mice (0.02 ± 0.01, mean ± SEM, $n = 3$ mice, $p < 0.001$, *U* test). In control mice, most terminal profiles in the neuropil of the molecular layer were small in size (0.5–1.0 μm in diameter), oval in shape, and in contact with single PC spines, i.e., one-to-one contact (Fig. 1*F*).

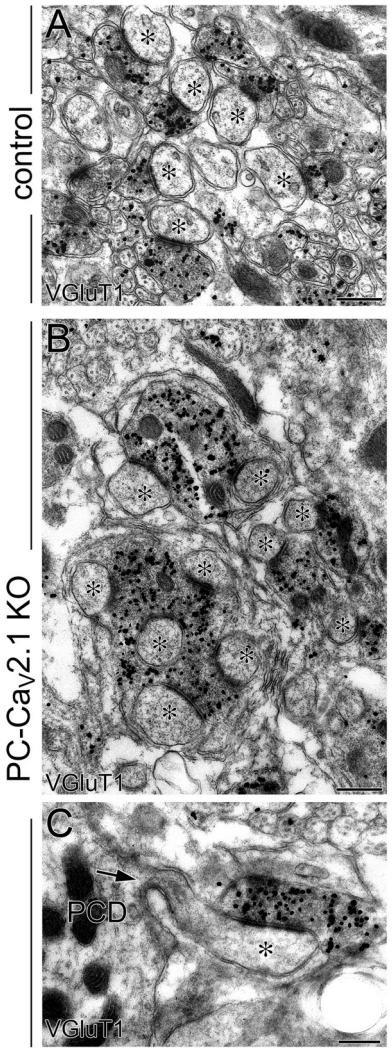

Figure 2. Multiple spine contact with enlarged PF terminals and proximal innervation of PFs in PC-$Ca_v2.1$ KO mice. Preembedding immunogold microscopy for VGluT1 in control (***A***) and PC-$Ca_v2.1$ KO (***B***, ***C***) mice. Asterisks indicate PC spines contacting to VGluT1(+) PF terminals. Arrow indicates a spine from PC dendrite (PCD). Scale bars, 500 nm.

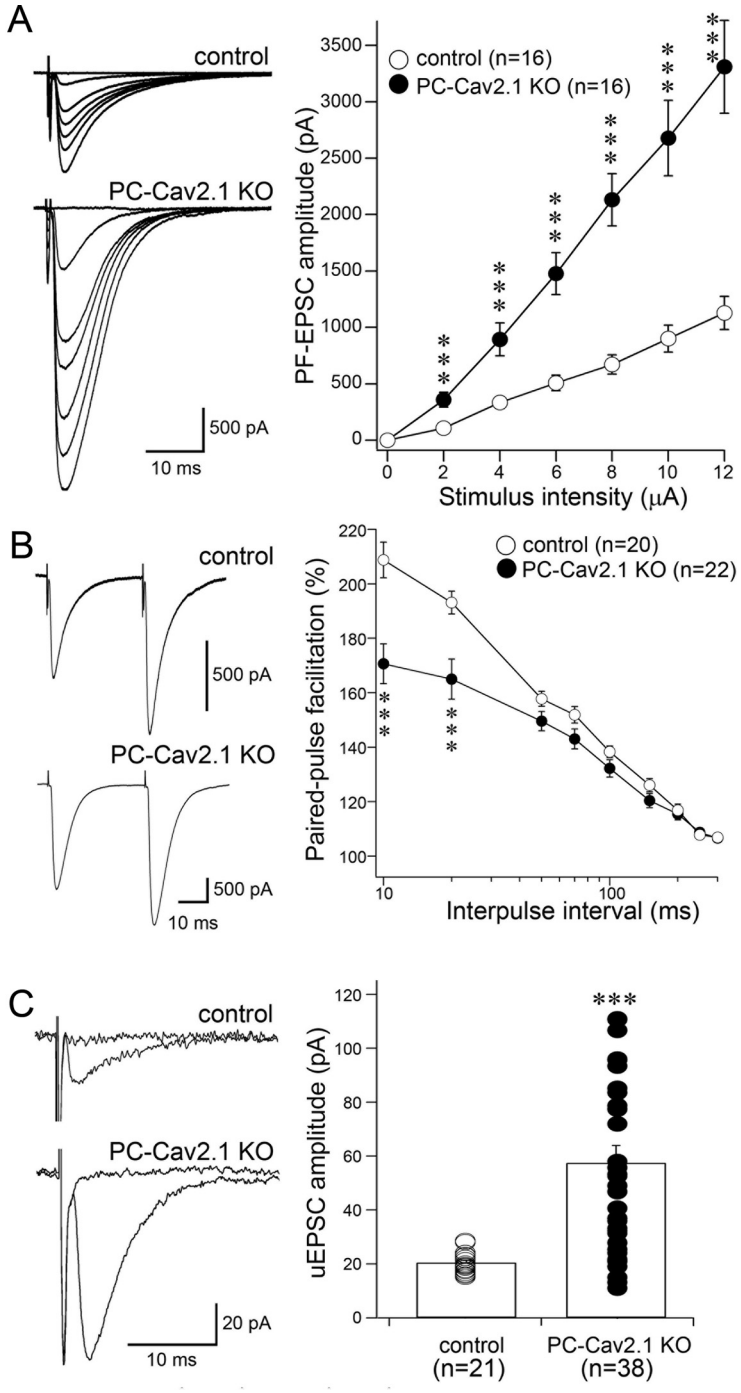

Figure 3. Enhanced PF-to-PC synapse transmission in PC-$Ca_v2.1$ KO mice. ***A***, Left, Representative traces of PF-EPSCs recorded at various stimulus intensities in the control (top) and the PC-Cav2.1 KO (bottom) PC. ***A***, Right, Averaged input–output relationship of PF-EPSCs in control (white circles; $n = 16$ PCs) and PC-$Ca_v2.1$ KO (black circles; $n = 16$ PCs) PCs. ***B***, Left, Representative traces of PF-EPSCs with an interpulse interval of 50 ms in control (top) and PC-Cav2.1 KO (bottom) PCs. ***B***, Right, Paired-pulse facilitation of PF-EPSCs in control (white circles; $n = 20$) and PC-$Ca_v2.1$ KO (black circles; $n = 22$) mice. The amplitude of the second response is expressed as the percentage of the first response and is plotted as a function of interpulse intervals. Stimulus pairs were applied at 0.5 Hz. ***C***, Left, Representative traces of PF response to a minimal intensity stimulation [unitary EPSC (uEPSC)] in control (top) and PC-Cav2.1 KO (bottom) PCs. ***C***, Right, Amplitudes of unitary EPSCs in control (white circles; $n = 21$) and PC-$Ca_v2.1$ KO (black circles; $n = 38$) mice. Six, six, and eight traces are averaged at a holding potential of −80 mV for ***A***, ***B***, and ***C***, respectively. ***$p < 0.001$, *U* test. Error bars indicate the SEM.

In contrast, terminal profiles in PC-$Ca_v2.1$ KO mice were remarkably enlarged (>1.0 μm in diameter) (Fig. 1*H*). These enlarged terminals were in contact with multiple PC spines, i.e., multiple contact, and often engulfed them (Fig. 1*H*, arrowheads), resulting in highly convoluted terminal contours. On single-electron micrographs, the fraction of terminal profiles forming multiple contact was 2.1 ± 0.1% in control mice and 26.7 ± 1.5% in PC-$Ca_v2.1$ KO mice, a significant difference ($n = 3$ mice, $p < 0.001$, *U* test). Despite the increased contact ratio, the density of asymmetrical synapses on PC spines was significantly decreased in PC-$Ca_v2.1$ KO mice (15.0 ± 2.8 per 100 μm^2 of neuropil area) compared with control mice (21.5 ± 0.7, $n = 3$ mice, $p < 0.05$, *U* test).

PF terminals were neurochemically identifiable by immunohistochemistry for VGluT1, a marker for PF terminals in the cerebellar molecular layer (Fremeau et al., 2001; Miyazaki et al., 2003; Figs. 1*I*,*J*, 2*A*–*C*). In control mice, VGluT1(+) puncta were uniformly fine, moderate in intensity, and densely distributed in the molecular layer (Fig. 1*I*). In contrast, they were sparse in PC-$Ca_v2.1$ KO mice, and a substantial fraction was apparently coarse and intense (Fig. 1*J*). By preembedding immunogold microscopy, the majority of terminals forming asymmetrical synapses on dendritic spines were labeled for VGluT1 in both types of mice, indicating that these asymmetrical synapses are PF–PC synapses. As expected, almost all PF–PC synapses in control mice had one-to-one contact, with a few being one-to-two contact between PF terminals and PC spines, and PF terminals were uniformly small and oval (Fig. 2*A*). In PC-$Ca_v2.1$ KO mice, however, some PF–PC synapses had such one-to-one contact, but others had enlarged PF terminals forming multiple contacts (Fig. 2*B*). Furthermore, we found that many ectopic spines on proximal dendrites were innervated by VGluT1(+) PF terminals (Fig. 2*C*). Therefore, the loss of $Ca_v2.1$ in PCs induces proximal expansion of PF territory and marked enlargement of PF terminals forming multiple contacts.

Electrophysiological properties of PF–PC synapses in PC-$Ca_v2.1$ KO mice

The altered synaptic morphology may affect electrophysiological properties of PF–PC synapses in PC-$Ca_v2.1$ KO mice. To address this issue, we recorded PF-EPSCs of PCs at P14–P21 and examined the input–output relationship of PF-EPSCs. Their amplitudes gradually increased with PF stimulus intensity in both control and PC-$Ca_v2.1$ KO mice (Fig. 3*A*), and there were no significant differences in the 10–90% rise time and decay time constant: the 10–90% rise time was 1.1 ±. 0.2 ms (mean ± SD; $n = 18$) and 1.1 ±. 0.5 ms ($n = 16$) in control and PC-$Ca_v2.1$ KO mice, respectively ($p = 0.29$, *U* test). The decay time constant was 5.9 ±. 2.0 ms ($n = 18$)

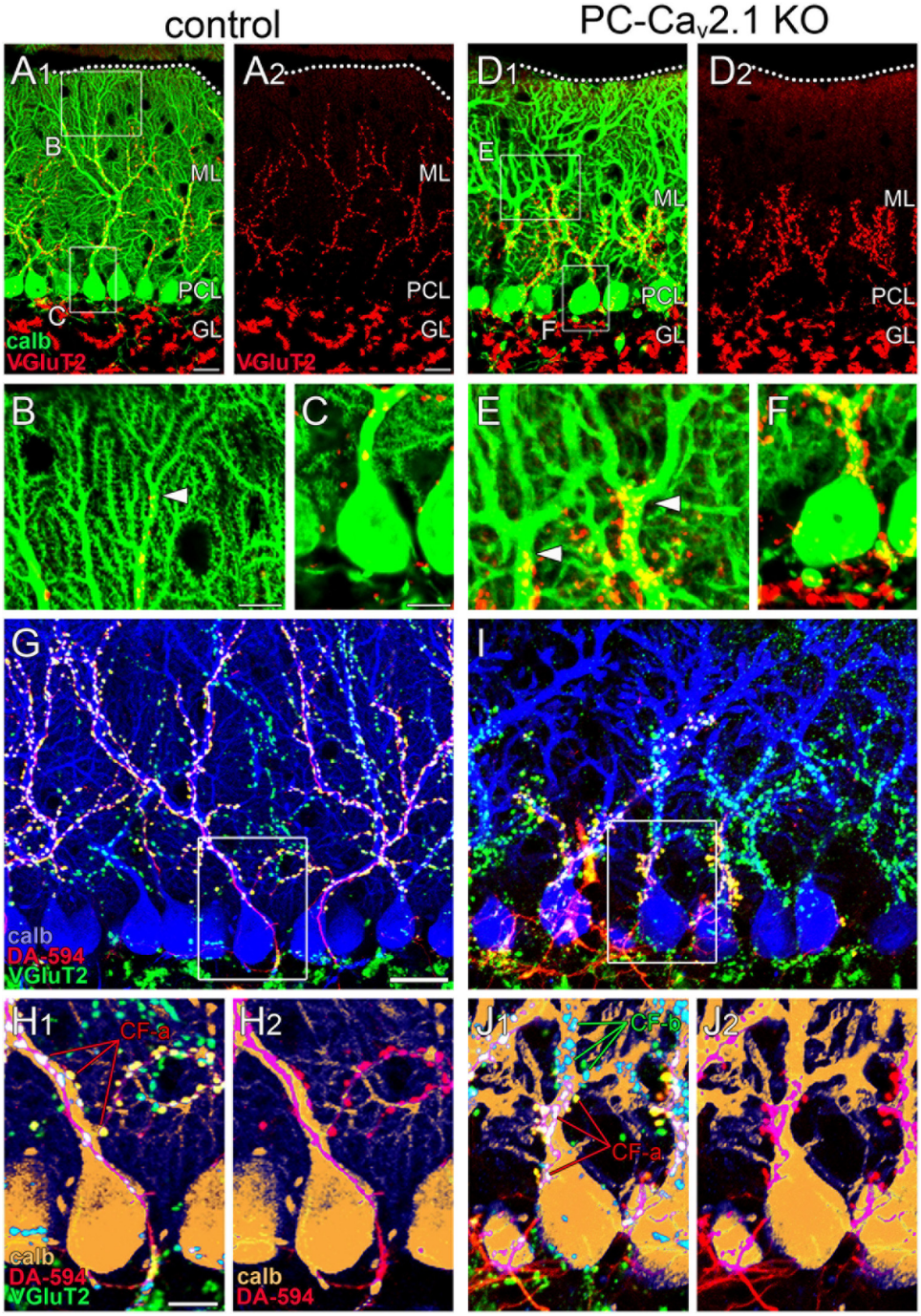

Figure 4. Regressed CF territory and multiple CF innervation in PC-$Ca_v2.1$ KO mice. ***A–F***, Double immunofluorescence for calbindin (green) and VGluT2 (red) in control (***A–C***) and PC-$Ca_v2.1$ KO (***D–F***) mice. Boxed regions in ***A*** and ***D*** are enlarged in ***B***, ***C***, ***E***, and ***F***. Dotted lines indicate the pia mater. Arrowheads in ***B*** and ***E*** indicate the distal tips of VGluT2(+) CF terminals along PC dendrites. ***G–J***, Triple fluorescent labeling for calbindin (blue in ***G***, ***I***; brown in ***H***, ***J***), VGluT2 (green), and anterograde tracer DA-594 injected into the inferior olive (red) in control (***G***, ***H***) and PC-$Ca_v2.1$ KO (***I***, ***J***) mice. Boxed regions in ***G*** and ***I*** are enlarged in ***H*** and ***J***, respectively. calb, calbindin; CF-a and CF-b, tracer(+)/VGluT2(+) or tracer(−)/VGluT2(+) CFs, respectively; GL, granule cell layer; ML, Molecular layer; PCL, Purkinje cell layer. Scale bars: ***A***, ***G***, 20 μm; ***B***, ***C***, ***H***, 10 μm.

and 5.6 ± 2.0 ms ($n = 16$) in control and PC-$Ca_v2.1$ KO mice, respectively ($p = 0.81$). However, PCs in PC-$Ca_v2.1$ KO mice displayed significantly larger PF-EPSC amplitudes than those in control mice at all stimulus intensities examined ($n = 16$ each; $p < 0.001$, at all stimulus intensities). These results suggest that PF-to-PC synaptic transmission is markedly enhanced in PC-Cav2.1 KO mice.

We further performed experiments to assess possible changes in the physiological properties of PF-EPSCs. We found that the paired-pulse ratio at interpulse intervals <50 ms was significantly smaller in PC-$Ca_v2.1$ KO mice than in control mice ($p < 0.001$), suggesting a higher presynaptic release probability in PC-$Ca_v2.1$ KO mice (Fig. 3*B*). Furthermore, by using minimal extracellular stimulation, we isolated EPSCs elicited by single PFs (unitary PF-EPSC). Small increments in a weak stimulation current often elicited an all-or-none excitation of a single axon, producing a unitary synaptic response (Bekkers and Clements, 1999). We found that the amplitudes of unitary EPSCs in PC-$Ca_v2.1$ KO PCs

were larger and more variable (57.5 ± 39.9 pA; $n = 38$) than those in control PCs (20.5 ± 3.8 pA; $n = 21$; Fig. 3*C*). Together, these results indicate that PF–PC synaptic transmission is enhanced in PC-$Ca_v2.1$KO mice, at least in part as a result of increases in the release probability from PF terminals and the number of contacts between individual PF terminals and PC spines (Fig. 2).

Regressed CF territory and multiple innervation at soma and basal dendrites

Next, we investigated the distribution patterns of CF terminals in the cerebellar molecular layer at P21 by double immunofluorescence for calbindin and VGluT2, a marker of CF terminals in the molecular layer (Fig. 4*A–F*). In control mice, CF terminals were distributed in the basal four-fifths of the molecular layer and extended up along proximal shaft dendrites until the border with distal spiny branchlets (Fig. 4*B*, arrowhead). In PC-$Ca_v2.1$ KO mice, CF terminals were irregular in shape and size, and their innervation stopped midway along proximal dendrites (Fig. 4*E*, arrowheads). This impaired innervation was reflected in a significant lowering of the mean height to the tips of VGluT2(+) terminals relative to the molecular layer thickness: 75.2 ± 0.7% in control mice and 52.2 ± 2.1% in PC-$Ca_v2.1$ KO mice (mean ± SEM, $n = 3$ mice, $p < 0.001$; *U* test). Around PC somata, VGluT2(+) CF terminals were rare in control mice (Fig. 4*C*) but frequent in PC-$Ca_v2.1$ KO mice (Fig. 4*F*). We counted the number of perisomatic CF terminals on the upper half of PC somata, in which most of the perisomatic CF terminals directly attach to the soma without glial intervention (Hashimoto et al., 2011; Ichikawa et al., 2011). The mean number of VGluT2(+) perisomatic terminals per 100 μm of the somatic surface was significantly higher in PC-$Ca_v2.1$ KO mice (2.4 ± 0.4) than in control mice (0.6 ± 0.1, mean ± SEM, $n = 3$ mice, $p < 0.05$, *U* test). In preembedding immunogold microscopy for VGluT2 (Fig. 5*A–C*), dendritic innervation by CFs was observed in both control and PC-$Ca_v2.1$ KO mice (Fig. 5*A*,*B*). Unlike PF terminals, no obvious changes were noted in the morphology of CF terminals. However, consistent with light microscopic observation, CF innervation to somatic spines was frequently observed in PC-$Ca_v2.1$ KO mice (Fig. 5*C*).

In PC-$Ca_v2.1$ KO mice, we recently demonstrated impaired functional strengthening of single winner CFs and severe persistence of multiple CF innervation (Hashimoto et al., 2011). In the present study, we confirmed this by using triple labeling with anterograde DA-594 tracer (Fig. 4*G–J*, red) and immunofluorescence for VGluT2 (Fig. 4*G–J*, green) and calbindin (Fig. 4*G*,*I*, blue, *H*,*J*, brown). In control mice, DA-594 and VGluT2 overlapped almost completely along dendritic trees of a given PC, displaying the typical anatomical pattern of CF monoinnervation (Fig. 4*G*,*H*). In PC-$Ca_v2.1$ KO mice, however, the proximal somatodendritic domain of a given PC was innervated by both DA-594(+)/VGluT2(+) and DA-594(−)/VGluT2(+) CFs (Fig. 4*I*,*J*). Thus, $Ca_v2.1$ KO in PCs leads to regressed CF territory down to basal dendrites and somata, at which portions multiple CFs of different neuronal origins form aberrant wiring patterns.

Normal synaptic structure and wiring in GC-$Ca_v2.1$ KO mice

To create a mouse model lacking presynaptic $Ca_v2.1$ at PF–PC synapses, we produced GC-$Ca_v2.1$ KO mice by crossing $Ca_v2.1$-floxed mice with E3CreN mice (Fig. 6*A*,*B*). Cre activity in E3CreN mice was examined using reporter mice and strong β-galactosidase staining was observed in the granular layer of the cerebellum, thalamus, olfactory bulb, and pontine nuclei at P21

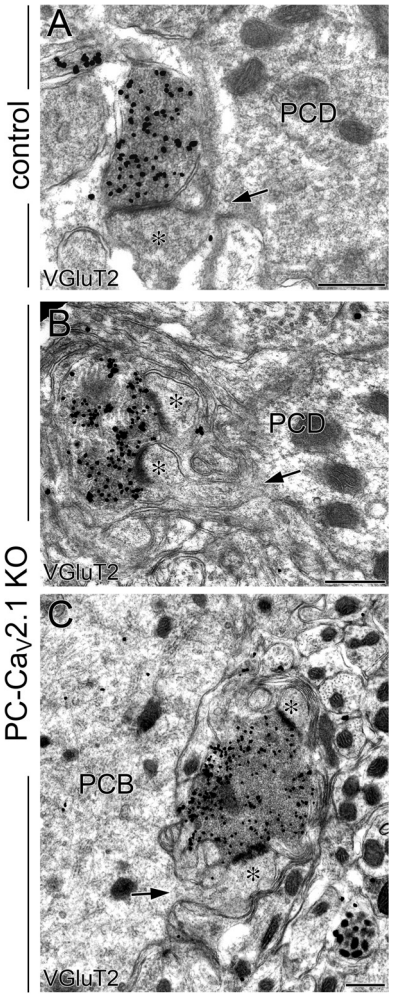

Figure 5. Somatic CF innervation in PC-$Ca_v2.1$ KO mice. Preembedding immunogold microscopy for VGluT2 (***A–C***) in control (***A***) and PC-$Ca_v2.1$ KO (***B***, ***C***) mice. Asterisks indicate PC spines in contact with VGluT2(+) CF terminals. Arrows indicate spines from PC dendrites (PCD) or PC bodies (PCB). Scale bars, 500 nm.

(Fig. 6*C*). At a higher magnification, β-galactosidase staining was observed in GCs but not in PCs or in molecular layer interneurons in the cerebellar cortex (Fig. 6*D*). We also observed weak staining in other brain regions, including the cerebral cortex, hippocampus, and brainstem. This staining pattern in reporter mouse brains faithfully reflected GluN2C mRNA expression (Watanabe et al., 1992; Mitani et al., 1998). Immunofluorescent signals for $Ca_v2.1$ were markedly reduced in the cerebellar cortex of GC-$Ca_v2.1$ KO mice (Fig. 6*E–H*) and were lost almost completely in that of global $Ca_v2.1$ KO mice (Fig. 6*I*,*J*). In control mice, tiny punctate clusters for $Ca_v2.1$ were associated with both VGluT1(+) PF terminals and VGluT2(+) CF terminals (Fig. 6*K*,*M*, arrowheads). In GC-$Ca_v2.1$ KO mice, however, $Ca_v2.1$ was lost in PF terminals (Fig. 6*L*, arrowheads), whereas $Ca_v2.1$ was detected in CF terminals (Fig. 6*N*, arrowheads) and shaft dendrites of PCs (PCD, Fig. 6*L*). Thus, $Ca_v2.1$ in PF terminals is selectively eliminated in the cerebellar cortex of GC-$Ca_v2.1$ KO mice.

In GC-$Ca_v2.1$ KO mice, none of the phenotypes observed in PC-$Ca_v2.1$ KO mice were observed. The size and histology of the cerebellum were normal, and the thickness and cell density in the granular layer were also normal (Fig. 7*A–C*). Furthermore, we found no hyperspiny transformation in the proximal dendrites

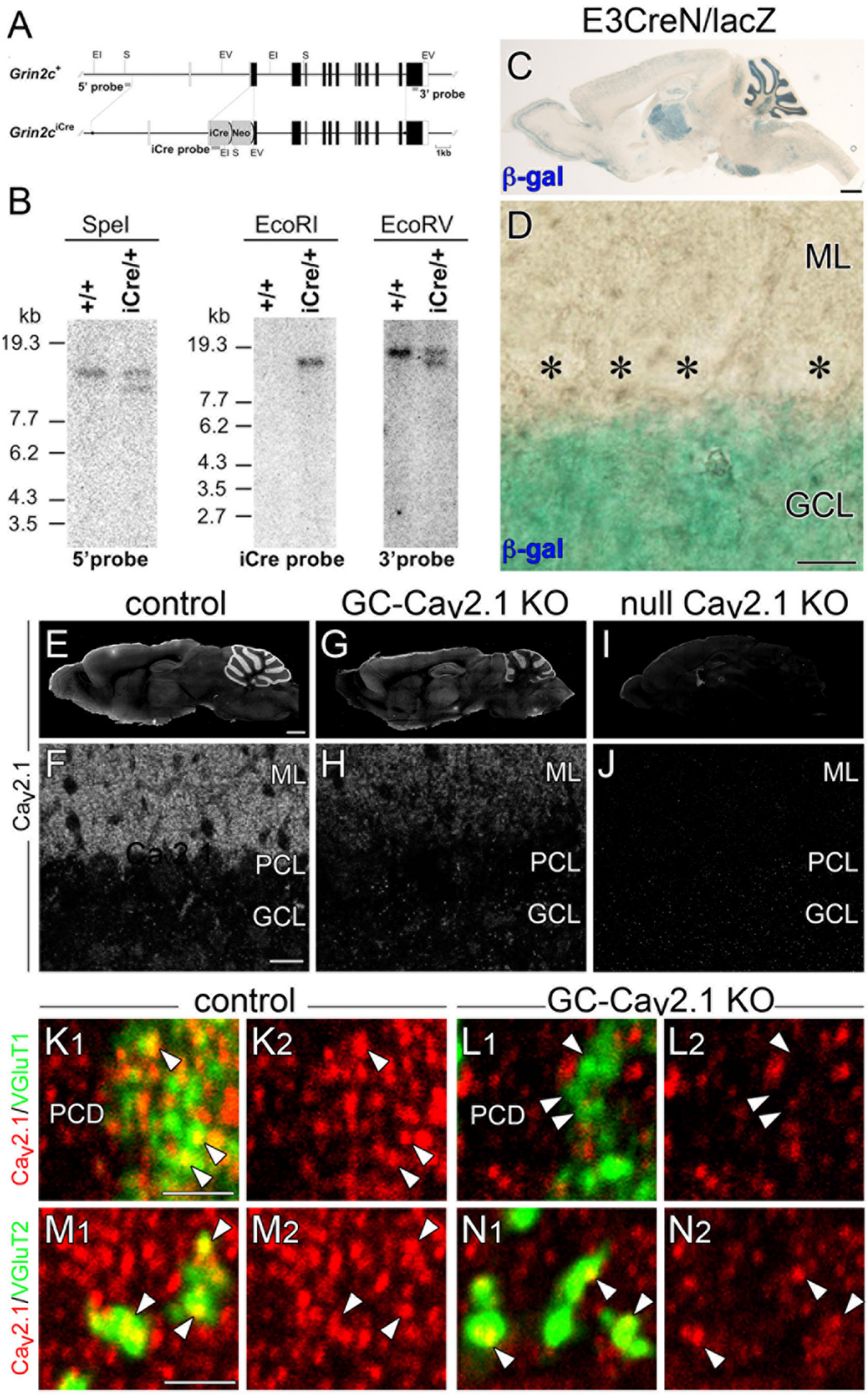

Figure 6. Production of mice with GC-specific $Ca_v2.1$ elimination. ***A***, Schematic representation of the GluN2C genomic DNA (*Grin2c* $^{+}$) and targeted genome (*Grin2c* ^{iCre}). The open and filled boxes indicate the noncoding and coding exons, respectively. The filled circles in the *Grin2c* ^{iCre} allele delineate the 5′ and 3′ termini of the targeting vector. The vector was constructed to insert an improved Cre recombinase gene (iCre) into the translational initiation site of the GluN2C gene in frame. The gray bars indicate the probes for Southern blot analysis. Two *frt* sequences (semicircles) are attached to remove the neomycin resistant gene (Neo). EI, EcoRI; EV, EcoRV; S, SpeI. ***B***, Southern blot analysis of the GluN2C wild-type (+/+) and targeted (iCre/+) genome. Left, SpeI-digested genomic DNA hybridized with 5′ probe; middle, EcoRI-digested DNA hybridized with iCre probe; right, EcoRV-digested DNA hybridized with 3′ probe. Positions of DNA size markers (kilobases) are indicated on the left. ***C***, ***D***, Cre recombinase activity induced by E3CreN in lacZ reporter mouse. β-Galactosidase staining (blue) of parasagittal brain section (***C***) and cerebellar cortex (***D***) at P21. Asterisks indicate PC bodies. ***E–J***, Immunofluorescence for $Ca_v2.1$ in control (***E***, ***F***), GC-$Ca_v2.1$ KO (***G***, ***H***), and global $Ca_v2.1$ KO (***I***, ***J***) mice. $Ca_v2.1$ immunoreactivity is selectively decreased in the cerebellar cortex of GC-$Ca_v2.1$ KO mice and disappears in the brain of global $Ca_v2.1$ KO mice. ***K–N***, Double immunofluorescence for $Ca_v2.1$ (red) with VGluT1 (green, ***K***, ***L***) or VGluT2 (green, ***M***, ***N***) (*Figure legend continues*.)

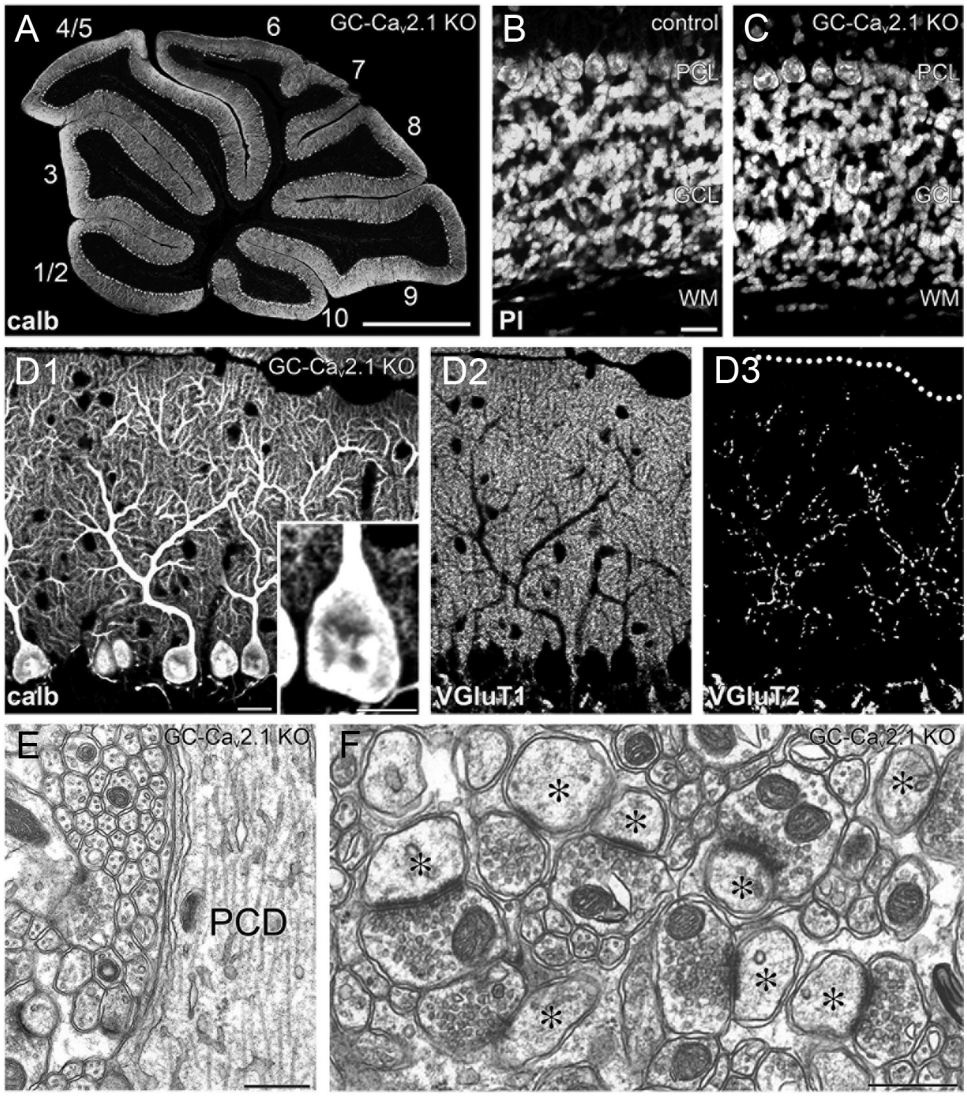

Figure 7. Normal synaptic wiring and structure in GC-$Ca_v2.1$ KO mice. ***A***, Immunofluorescence for calbindin in the cerebellum of GC-$Ca_v2.1$ KO mice. The lobule number is indicated by numerals 1–10. ***B***, ***C***, Normal histology of the granular layer, as shown by propidium iodide (PI) staining in control (***B***) and GC-$Ca_v2.1$ KO (***C***) mice. ***D***, Triple immunofluorescence for calbindin (***D*$_1$**), VGluT1 (***D*$_2$**), and VGluT2 (***D*$_3$**) in GC-$Ca_v2.1$ KO mice. ***E***, ***F***, Electron micrographs showing smooth surface of PC shaft dendrites (***E***) and normal morphology of PF–PC synapses (***F***). GCL, Granular cell layer; ML, molecular layer; PCD, Purkinje cell dendrite; PCL, Purkinje cell layer; WM, white matter. Scale bars: ***A***, 1 mm; ***B***, ***D*$_1$**, 20 μm; ***D*$_1$**, inset, 10 μm; ***E***, ***F***, 500 nm.

and somata of PCs (Fig. 7D_1,E), no enlargement or multiple contact of PF terminals (Fig. 7D_2,F), and no regressed CF territory (Fig. 7D_3). These results demonstrate that the loss of postsynaptic, but not presynaptic, $Ca_v2.1$ at PC synapses is responsible for the aberrant synaptic structure and wiring defects in PCs of $Ca_v2.1$ mutant mice (Miyazaki et al., 2004).

Progressive and patterned PC degeneration

In PC-$Ca_v2.1$ KO mice, the size of the cerebellum was further reduced from P21 to maturity, suggestive of neuronal degeneration. We examined the mechanism of this size reduction by calbindin immunofluorescence using horizontal cerebellar sections. In this section plane, a fan-like dendritic tree observed in the parasagittal plane (Fig. 4A,D) is visible as a single straight bar traversing the molecular layer (Fig. 8B,D). At P14, dendritic bars were densely arranged in a palisade-like pattern in both types of mice (Fig. 8A–D). This feature was maintained in control and GC-$Ca_v2.1$ KO mice at P21, P28, and P35 (data not shown). In PC-$Ca_v2.1$ KO mice, PCs started to decrease at P21 (Fig. 8E,F) and further decreased thereafter (Fig. 8G–J). By electron microscopy, the soma and dendrites of PCs in PC-$Ca_v2.1$ KO mice at P28 exhibited degenerative features, including somatic shrinkage, darkened cytoplasm, increased electron-dense materials, and extensive accumulation of mitochondria (Fig. 9C,D). No such degenerative features were observed in PCs of control mice (Fig. 9A,B) or in PCs and GCs of GC-$Ca_v2.1$ KO mice (data not shown). At P35, PC somata and dendrites were rarely encountered in the cerebellar cortex of PC-$Ca_v2.1$ KO mice (data not shown). Thus, it appears that PCs degenerate progressively in PC-$Ca_v2.1$ KO mice.

We noticed that PC degeneration in PC-$Ca_v2.1$ KO mice occurred more in anterior lobules than in posterior lobules and that

←

(*Figure legend continued.*) in control (***K***, ***M***) and GC-$Ca_v2.1$ KO (***L***, ***N***) mice. Note the disappearance of $Ca_v2.1$ in VGluT1(+) PF terminals (arrowheads in ***K***, ***L***) but not in VGluT2(+) CF terminals (arrowheads in ***M***, ***N***) or shaft dendrites of PCs (PCD) in GC-$Ca_v2.1$ KO mice. β-gal, β-galactosidase; GCL, Granular cell layer; ML, molecular layer; PCL, Purkinje cell layer. Scale bars: ***C***, ***E***, 1 mm; ***D***, ***F***, 20 μm; ***K***, ***M***, 2 μm.

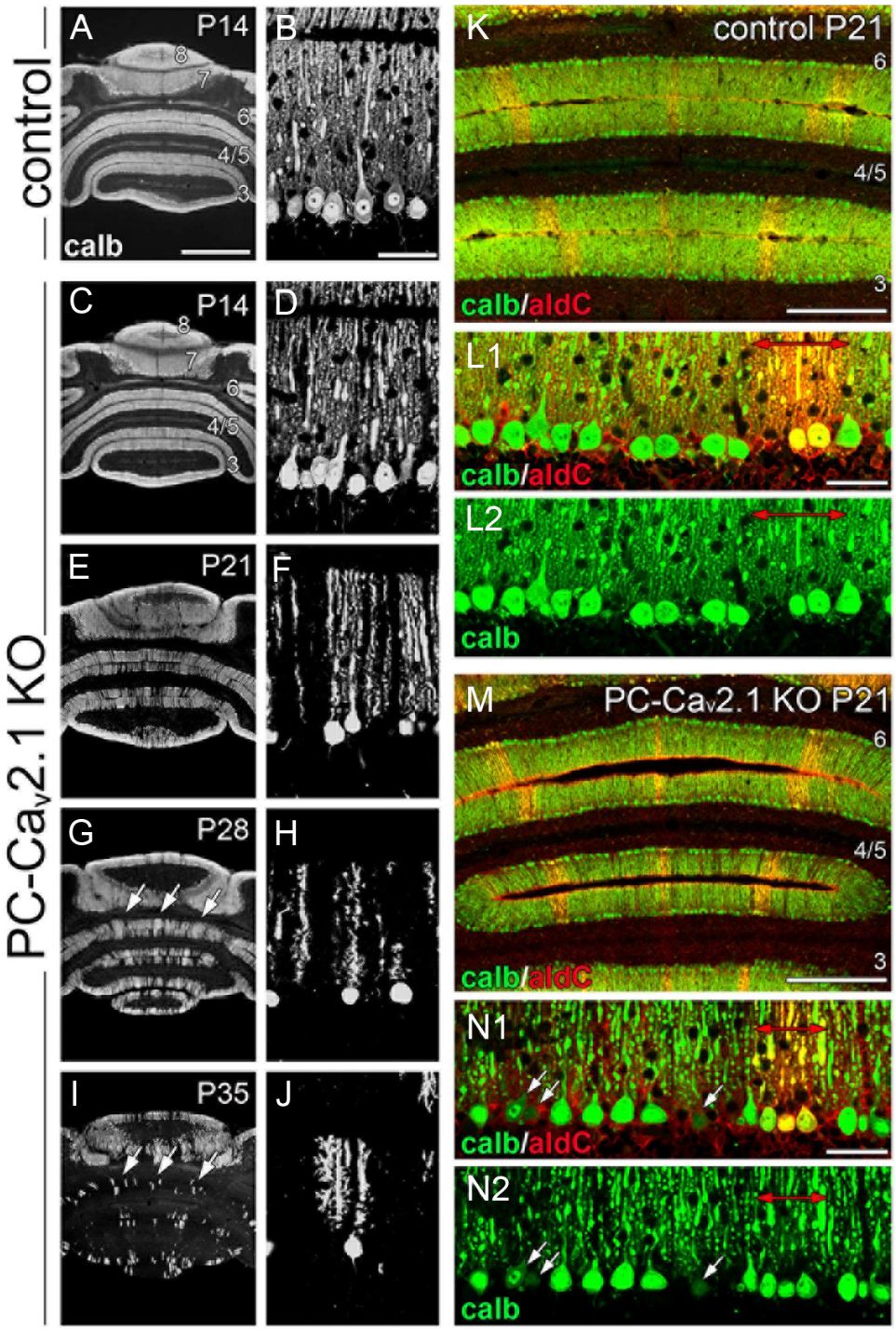

Figure 8. Progressive PC loss in aldolase C(−) cerebellar compartments of PC-$Ca_v2.1$ KO mice. ***A–J***, Immunofluorescence for calbindin in horizontal cerebellar sections of control mice at P14 (***A***, ***B***) and PC-$Ca_v2.1$ KO mice at P14 (***C***, ***D***), P21 (***E***, ***F***), P28 (***G***, ***H***), and P35 (***I***, ***J***). Arrows in ***G*** and ***I*** indicate banded clusters of remaining PCs. ***K–N***, Double immunofluorescence for calbindin (calb; green) and aldolase C (aldC; red) in control (***K***, ***L***) and PC-$Ca_v2.1$ KO (***M***, ***N***) mice at P21. Red arrows in ***L*** and ***N*** indicate aldolase C(+) compartments. Arrows in ***N*** indicate that PC somata with lowered calbindin immunofluorescence were preferentially distributed in aldolase C(−) compartments. Numerals 3– 8 indicate the lobule number. Scale bars: ***A***, 1 mm; ***B***, ***L***, ***N***, 50 μm; ***K***, ***M***, 500 μm.

clusters of surviving PCs showed banded or striped patterns (Fig. 8*G*,*I*, arrows). This pattern of PC degeneration is known to occur in aldolase C/zebrin II antigen(−) cerebellar compartments of spontaneous $Ca_v2.1$ mutant mice (so-called *leaner* and *tottering* mice; Herrup and Wilczynski, 1982; Heckroth and Abbott, 1994; Sawada et al., 2009). To confirm this, double immunofluorescence for calbindin and aldolase C was applied to control and PC-$Ca_v2.1$ KO mice at P21 (Fig. 8*K–N*). In both types of mice (Fig. 8*L*,*N*), aldolase C was intense in PC subsets, which formed symmetrical arrays of parasagittal compartments across the cerebellum (Fig. 8*K*,*M*). In PC-$Ca_v2.1$ KO mice, decreased calbindin immunoreactivity was discernable in PCs located within aldolase C(−) compartments (Fig. 8*N*, white arrows). Thereafter, the decrease or loss of calbindin signals became overwhelming in aldolase C(−) compartments and also occurred mildly in aldolase C(+) compartments (Fig. 8*G*, I). Therefore, $Ca_v2.1$ ab-

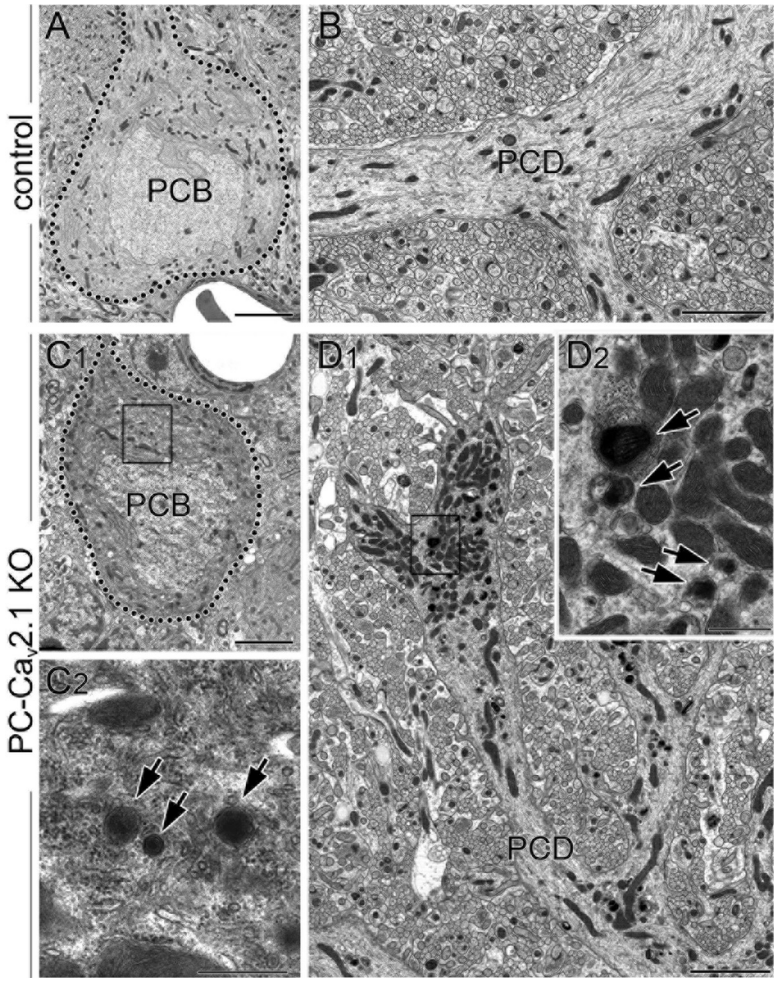

Figure 9. Degenerative features of PCs in PC-$Ca_v2.1$ KO mice. Electron micrographs showing cell bodies (PCB; ***A***, ***C***) and shaft dendrites of PCs (PCD; ***B***, ***D***) in control (***A***, ***B***) and PC-$Ca_v2.1$ KO (***C***, ***D***) mice at P28. In ***A*** and ***C***, the outline of PC somata is indicated by dotted lines. Boxed region in C_1 and D_1 are enlarged in C_2 and D_2, respectively. Arrows indicate electron-dense materials in PC-$Ca_v2.1$ KO PCs. Scale bars: ***A***, ***B***, C_1, D_1, 3 μm; C_2, D_2, 500 nm.

lation in PCs causes patterned PC degeneration, which starts in the third postnatal week and occurs preferentially in aldolase C(−) compartments.

Blurred reciprocity of PLCβ3 and PLCβ4 expression

In addition to aldolase C, several other molecules are known to display banded patterns of expression in PC populations (Hawkes, 1997; Hawkes and Eisenman, 1997; Herrup and Kuemerle, 1997; Larouche and Hawkes, 2006). Of these, two isoforms of phospholipase Cβ, PLCβ3 and PLCβ4, are expressed in patterns reciprocal to each other (Kano et al., 1998; Nomura et al., 2007), with PLCβ3 predominating in aldolase C(+) compartments and PLCβ4 in aldolase C(−) ones (Sarna et al., 2006). We examined PLCβ3 and PLCβ4 expression in horizontal cerebellar sections to test whether their compartmentalized expression was affected in PC-$Ca_v2.1$ KO mice (see Figs. 10–12).

Double immunofluorescence for PLCβ3 and PLCβ4 at P21 revealed that wide PLCβ4-dominant compartments in the anterior lobules and wide PLCβ3-dominant compartments in the posterior lobules were well preserved in both types of mice (Fig. 10*A*,*C*). Figure 10*F* shows an example of the anterior lobules in control mice, in which narrow PLCβ3-dominant compartments ($P1^+$, $P2^+$, and $P3^+$) are separated by wide PLCβ4-dominant compartments ($P1^-$ and $P2^-$). At high magnifications, however, altered expression patterns were evident between the two groups (Fig. 10*B*,*D*). In control mice, each dendritic bar was predominantly labeled for either PLCβ3 or PLCβ4, never for both, and the boundary of their compartments was sharply defined at the cellular level (Fig. 10*B*). In PC-$Ca_v2.1$ KO mice, the boundary was obscured by occasional coexpression of PLCβ3 and PLCβ4 in the same PCs at peri-boundary regions (Fig. 10*D*). To quantitatively evaluate this altered banding, we measured the width of PLCβ3-dominant, PLCβ4-dominant, and PLCβ3/4-coexpressing compartments in cerebellar compartments $P1^+$, $P1^-$, $P2^+$, $P2^-$, and $P3^+$ of the lobules 3–6. The relative width was comparable for PLCβ3-dominant compartments (Fig. 10*E*, green bars) but significantly decreased for PLCβ4-dominant compartments in PC-$Ca_v2.1$ KO mice (red bars). Clearly, the fractional decrease of PLCβ4-dominant compartments was comparable with the aberrant increase of PLCβ3/4-coexpressing compartments (yellow bars). Therefore, the blurred cerebellar banding is likely attributable to ectopic expression of PLCβ3 in PCs of PLCβ4-dominant compartments.

Furthermore, altered banding was evident in somatic PLCβ immunolabeling. In control PCs, PLCβ3 was moderate in perikarya of PLCβ3-dominant PCs, whereas PLCβ4 was very low in perikarya of PLCβ4-dominant PCs (Fig. 10*B*) (Nakamura et al., 2004; Nomura et al., 2007). In PC-$Ca_v2.1$ KO mice, PLCβ3 and PLCβ4 were intensified to various degrees in the perikarya of PCs (Fig. 10*D*). Here again, the intensification of perikaryal PLCβ4 labeling appeared to follow the border of compartments in control mice (Fig. 10B_3 vs 10D_3), whereas the intensification of perikaryal PLCβ3 labeling apparently extended beyond the border (Fig. 10B_2 vs 10D_2). All these changes were also observed in the posterior lobules (data not shown). Thus, $Ca_v2.1$ elimination in PCs not only blurs the reciprocity of PLCβ3 and PLCβ4 expression but also affects their intracellular distribution.

Posttranscriptional modification of PLCβ3 expression during early postnatal period

Next, we investigated the developmental profile of this blurred reciprocity during the early postnatal period. In control mice, banded expression of PLCβ4 was already seen at P7 (Fig. 11A_2), and it was maintained thereafter (Fig. 11B_2,C_2). This early onset of PLCβ4 banding and its continuity to adulthood are consistent with a previous study (Marzban et al., 2007). Conversely, PLCβ3 was homogeneously distributed throughout the molecular layer at P7 (Fig. 11A_1). Banded pattern of PLCβ3 expression became discernible at P14 by downregulation of PLCβ3 in PLCβ4-dominant compartments (Fig. 11B_1). However, PLCβ3 banding at P14 was still immature, because PLCβ3-dominant compartments were wider and less sharply defined than those at later stages. Moreover, insufficient downregulation of PLCβ3 in

PLCβ4-dominant compartments produced transient ectopic bands at P14 (Fig. 11B_1, arrowheads). Typical adult-pattern PLCβ3 banding, which precisely alternates with PLCβ4 banding, was completed at P21 (Fig. 11C_1).

In PC-$Ca_v2.1$ KO mice, spatiotemporal profiles of PLCβ4 banding closely mirrored those in control mice (Fig. 11D_2,E_2,F_2), and the homogeneous distribution of PLCβ3 at P7 was also similar. However, PLCβ3 banding was less clear in PC-$Ca_v2.1$ KO mice at P14 and P21 than in age-matched control mice (Fig. 11E_1,F_1). This obscurity was assessed quantitatively by measuring the gray density of fluorescent signals for PLCβ3 or PLCβ4 in the molecular layer and calculating the relative intensity gap of PLCβ3 between PLCβ3-strong and PLCβ3-weak compartments (Fig. 11*I*) and the relative intensity gap of PLCβ4 between PLCβ4-strong and PLCβ4-weak compartments (Fig. 11*J*). Compared with control mice, the relative intensity gap in PC-$Ca_v2.1$ KO mice was significantly reduced for PLCβ3 at P14 and P21 (Fig. 11*I*), whereas no significant changes were observed for PLCβ4 (Fig. 11*J*). This phenotype was not found in GC-$Ca_v2.1$ KO mice (Fig. 11*G*), but it was present in global $Ca_v2.1$ KO mice (Fig. 11*H*). Therefore, PLCβ3 banding develops its precise reciprocity to the preexisting PLCβ4 banding during the second and third postnatal weeks in normal development, and the elimination of $Ca_v2.1$ in PCs impairs this process.

Whether the impaired reciprocity occurred at the transcription level was tested by double fluorescent *in situ* hybridization (FISH) for PLCβ3 and PLCβ4 mRNAs (Fig. 12). The specificity of FISH signals was checked by reciprocal patterns of PC labeling with the use of antisense riboprobes (Fig. 12*A*,*C*) and by blank labeling with the sense riboprobes (Fig. 12*B*,*D*). Similarly to immunohistochemical patterns, PCs dominantly expressing PLCβ3 mRNA (Fig. 12*E*,*G*, β3) or PLCβ4 mRNA (Fig. 12*E*,*G*, β4) formed narrow or wide bands, respectively, in the anterior lobules. At a high magnification, many PCs strongly expressed either PLCβ3 mRNA (Fig. 12*F*,*H*, green arrowheads) or PLCβ4 mRNA (red arrowheads). To our surprise, some PCs in peri-boundary regions expressed both mRNAs at high levels in both control and PC-$Ca_v2.1$ KO mice (yellow arrowheads). Taking these results together, it appears that a crude map of PLCβ3 and PLCβ4 compartments is determined at the transcription level, but their precise reciprocity appears to be acquired through $Ca_v2.1$-mediated post-transcriptional modification, particularly modification of PLCβ3 expression.

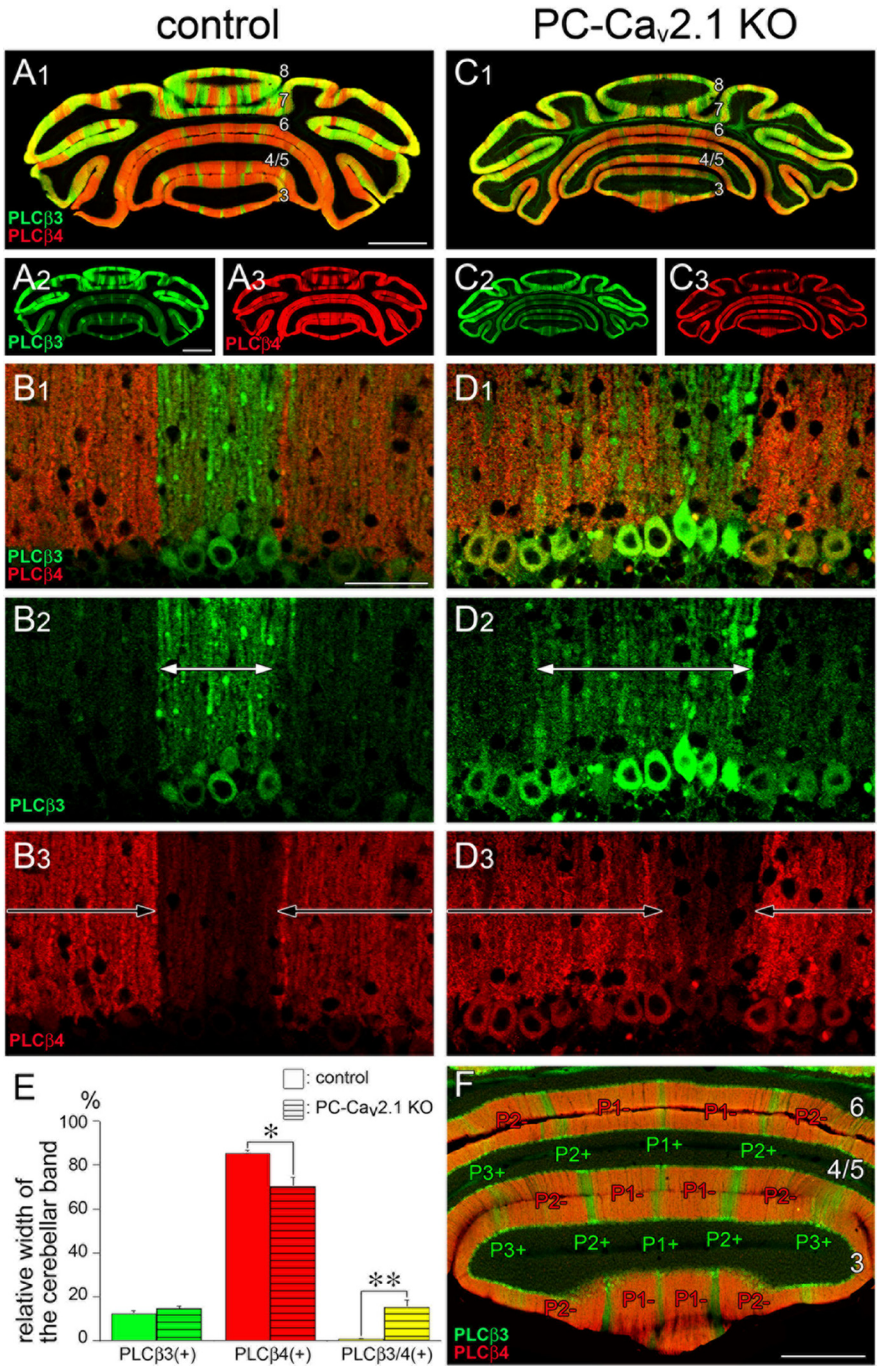

Figure 10. The sharp boundary in reciprocal distribution of PLCβ3 and PLCβ4 immunoreactivities in control mice is impaired in PC-$Ca_v2.1$ KO mice. ***A–D***, ***F***, Double immunofluorescence for PLCβ3 (green) and PLCβ4 (red) in horizontal cerebellar sections of control (***A***, ***B***, ***F***) and PC-$Ca_v2.1$ KO (***C***, ***D***) mice at P21. White and black arrows in ***B*** and ***D*** indicate cerebellar compartments dominantly expressing PLCβ3 or PLCβ4, respectively. Numerals 3–8 indicate the lobule number. In ***F***, the width of the cerebellar band was measured at the molecular layer compartments P1$^+$, P1$^-$, P2$^+$, P2$^-$, and P3$^+$ of lobules 3–6. ***E***, Histograms showing the width of PLCβ3-dominant (green), PLCβ4-dominant (red), and PLCβ3/4-double dominant (yellow) bands relative to the width of the total cerebellar bands measured. Open and striped bars indicate control and PC-$Ca_v2.1$ KO mice, respectively. The values for PLCβ3-dominant bands are as follows: 12.3 $\pm$ 1.4% in control and 14.6 $\pm$ 1.3% in PC-$Ca_v2.1$ KO mice, $p = 0.25$; PLCβ4-dominant bands, 85.6 $\pm$ 1.2% in control and 70.2 $\pm$ 4.0% in PC-$Ca_v2.1$ KO mice, $p < 0.05$; PLCβ3/4-double dominant bands, 0.8 $\pm$ 0.2% in control and 15.2 $\pm$ 3.4% in PC-$Ca_v2.1$ KO mice, $p < 0.01$ (mean $\pm$ SEM, $n = 3$ mice, *U* test). *$p < 0.05$; **$p < 0.01$. Scale bars: ***A***, 1 mm; ***B***, 50 μm; ***F***, 500 μm.

Altered banded expression of glutamate transporter EAAT4

Finally, we examined whether such alteration also happens to other compartment markers in the cerebellum. To this end, we chose the glutamate transporter EAAT4, whose banding patterns coincide with those of aldolase C and PLCβ3 (Nagao et al., 1997; Dehnes et al.,

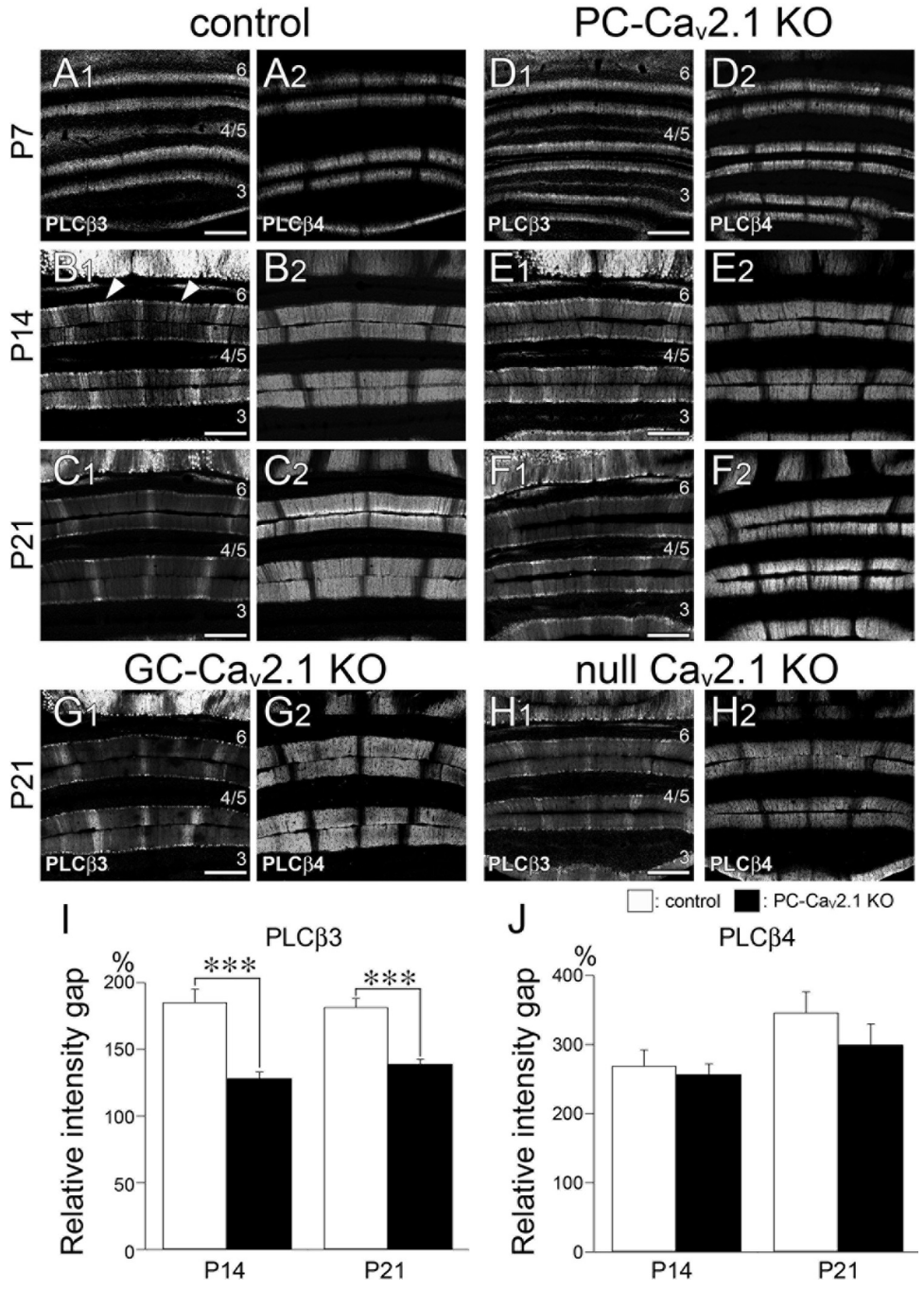

Figure 11. Impaired postnatal downregulation of PLCβ3 immunoreactivity in aldolase C/zebrin II-negative compartments of PC-$Ca_v2.1$ KO mice. ***A–H***, Immunofluorescence for PLCβ3 (***A_1–H_1***) and PLCβ4 (***A_2–H_2***) in control (***A–C***), PC-$Ca_v2.1$ KO (***D–F***), GC-$Ca_v2.1$ KO (***G***), and global $Ca_v2.1$ KO (***H***) mice at P7 (***A***, ***D***), P14 (***B***, ***E***), and P21 (***C***, ***F***, ***G***, ***H***). ***I***, ***J***, Histograms showing the relative intensity gap of PLCβ3 (***I***) or PLCβ4 (***J***) immunoreactivity between intensely labeled and weakly labeled compartments. The values for PLCβ3 are as follows: 185.4 $\pm$ 9.9% in control and 128.3 $\pm$ 4.6% in PC-$Ca_v2.1$ KO mice at P14, $p < 0.001$; 181.7 $\pm$ 6.6% in control and 139.1 $\pm$ 3.6% in PC-$Ca_v2.1$ KO mice at P21, $p < 0.0001$. The values for PLCβ4 are as follows: 269.1 $\pm$ 22.3% in control and 257.0 $\pm$ 15.0% in PC-$Ca_v2.1$ KO mice at P14, $p = 0.76$; 346.3 $\pm$ 29.9% in control and 299.7 $\pm$ 30.2% in PC-$Ca_v2.1$ KO mice at P21, $p = 0.17$ (mean $\pm$ SEM, $n = 3$ mice, *U* test). Numerals 3–6 indicate the lobule number. ***$p < 0.001$. Scale bars, 100 μm.

1998; Nomura et al., 2007). In double immunofluorescence for EAAT4 and aldolase C at P21, control mice clearly showed banded expression of EAAT4 (Fig. 13A_1), whereas it was less clear in PC-$Ca_v2.1$ KO mice (Fig. 13B_1). At a high magnification, EAAT4-dominant compartments were closely overlapped with aldolase C(+) compartments in control mice (Fig. 13*C*, double-headed arrows). In PC-$Ca_v2.1$ KO mice, EAAT4-dominant compartments (Fig. 13D_2, double-headed arrows) were broadened and obscured compared with aldolase C(+) compartments (Fig. 13D_3, double-headed arrows). The altered banding of EAAT4 expression was quantitatively confirmed in PC-$Ca_v2.1$ KO mice by observing a significant increase in the relative width of EAAT4-dominant bands and a significant decrease in the relative intensity gap of EAAT4 between EAAT4-strong and EAAT4-weak bands (Fig. 13*E*,*F*, left). No such quantitative differences were observed for aldolase C expression (Fig. 13*E*,*F*, right). Therefore, PC-specific elimination of $Ca_v2.1$ also affects the boundary of compartmental expression of the EAAT4.

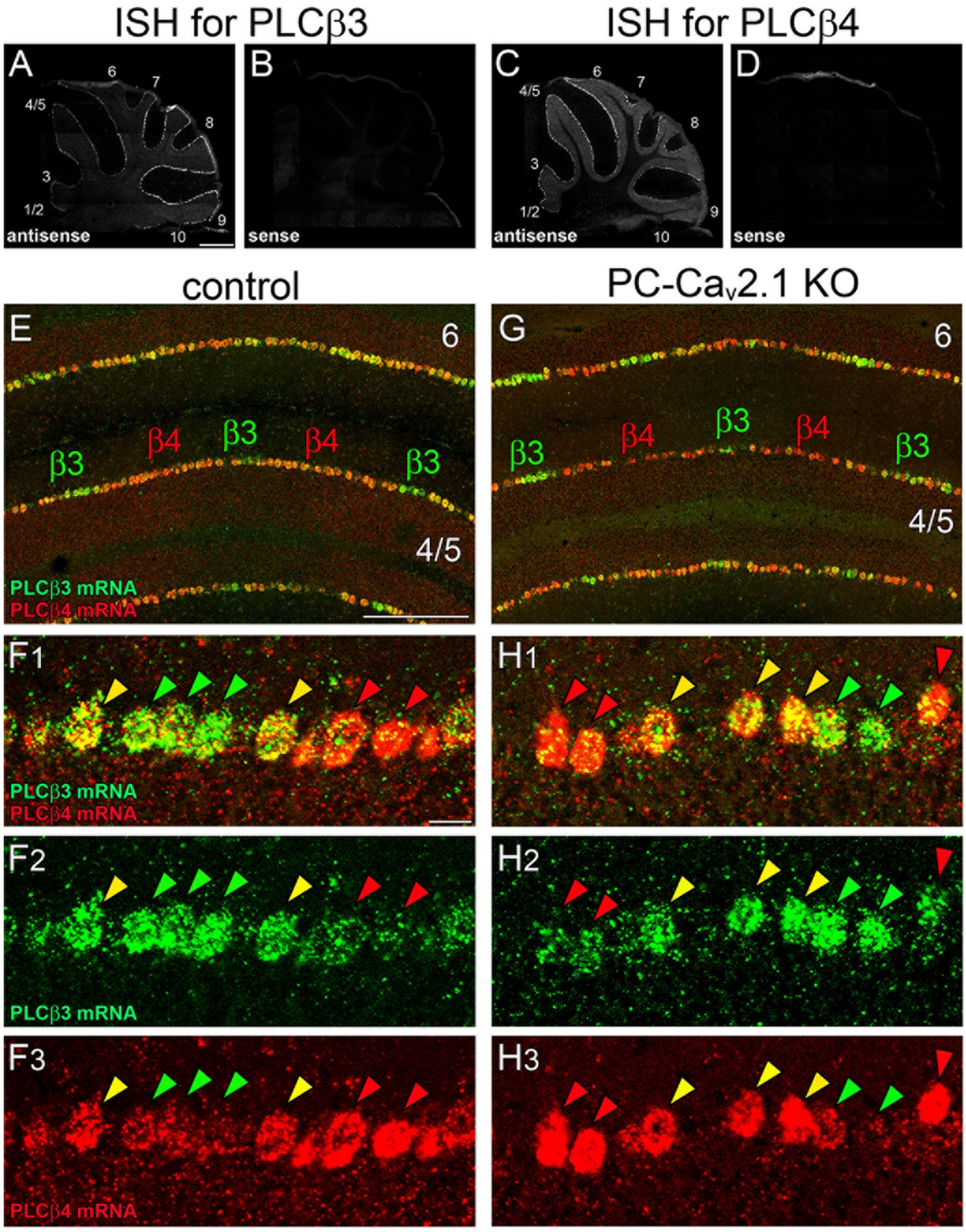

Figure 12. Blurred boundary of cerebellar compartments dominantly expressing PLCβ3 or PLCβ4 mRNA in both control and PC-$Ca_v2.1$ KO mice. ***A–D***, Specificity of riboprobes for PLCβ3 and PLCβ4 is indicated by reciprocal labeling of PC subsets with the use of antisense probes (***A***, ***C***) and blank labeling with the use of sense probes (***B***, ***D***). ***E–H***, Double FISH for PLCβ3 (green) and PLCβ4 (red) mRNAs in horizontal cerebellar sections of control (***E***, ***F***) and PC-$Ca_v2.1$ KO (***G***, ***H***) mice. In both types of mice, PC subsets dominantly expressing PLCβ3 (β3, green arrowheads) and PLCβ4 (β4, red arrowheads) grossly alternate, but PCs highly expressing both isoforms intervene between them (yellow arrowheads). Numerals 1–10 indicate the lobule number. Scale bars: ***A***, 500 μm; ***E***, 20 μm; ***F***$_1$, 100 μm.

Discussion

Development of excitatory PC wiring is controlled by molecular mechanisms mediating synaptic activity and connectivity, including the pore-forming subunit $Ca_v2.1$ of P/Q-type Ca^{2+} channels (Miyazaki and Watanabe, 2011; Watanabe and Kano, 2011). Although somatodendritic $Ca_v2.1$ in PCs is a major source of Ca^{2+} transient that contributes to the firing and waveform of action potentials, $Ca_v2.1$ is also a major presynaptic Ca^{2+} channel involved in transmitter release in the brain (Mintz et al., 1992, 1995). To specify the role of presynaptic and postsynaptic P/Q-type Ca^{2+} channels, we produced PC-$Ca_v2.1$ KO and GC-$Ca_v2.1$ KO mice in the present and previous studies (Hashimoto et al., 2011). Here we have shown that $Ca_v2.1$ elimination in PCs, but not in GCs, leads to impaired heterosynaptic competition between PFs and CFs on PCs, progressive and patterned degeneration of PCs, and blurred expression of PLCβ3 and EAAT4 around compartmental boundaries of PCs.

Postsynaptic $Ca_v2.1$ regulates competitive excitatory wiring in PCs

Various defects have been observed in excitatory wiring of PCs in global $Ca_v2.1$ KO mice and spontaneous $Ca_v2.1$ mutant mice, including proximal expansion of PF territory, enlargement of PF

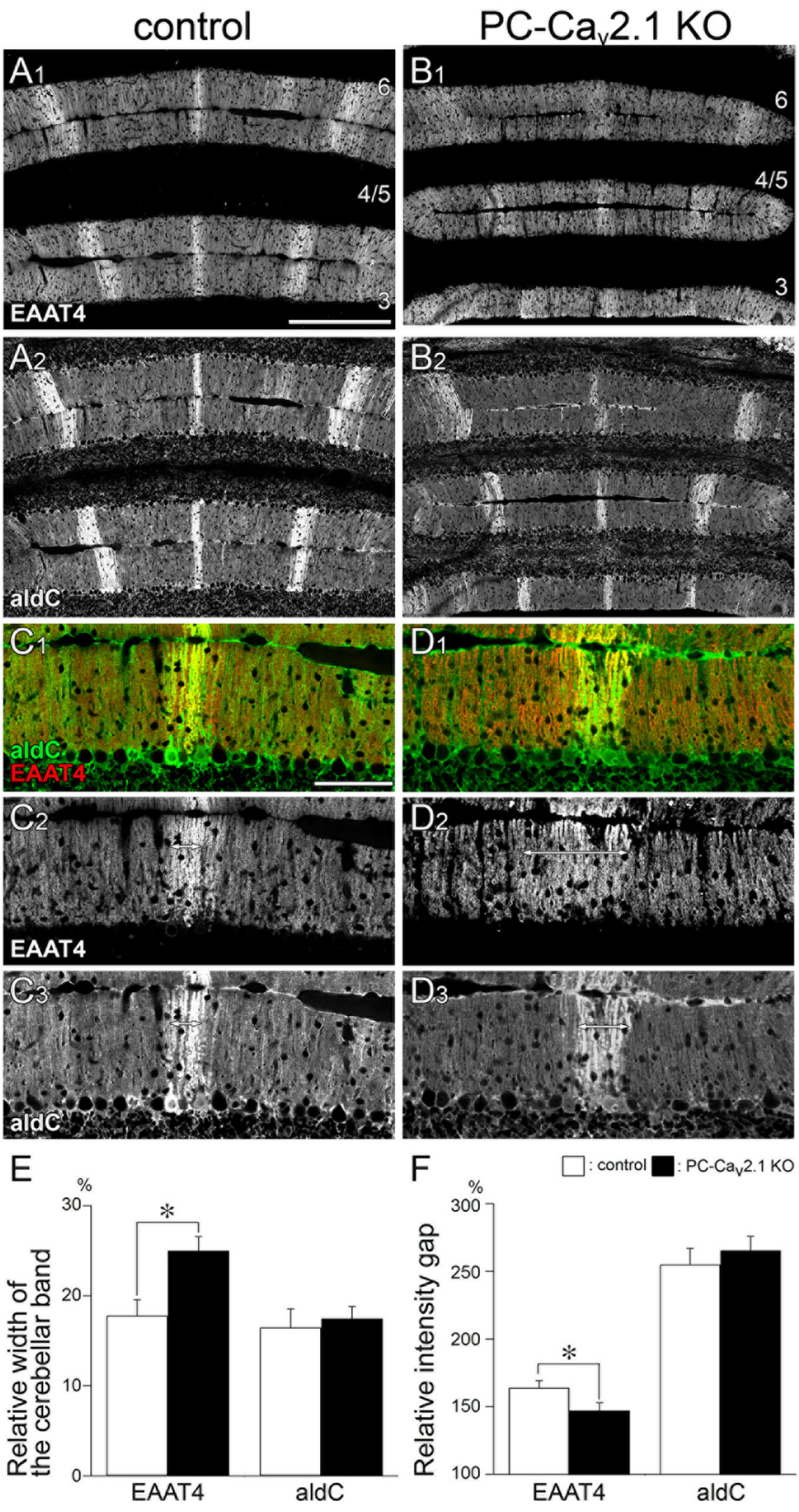

Figure 13. Altered boundary for EAAT4 cerebellar compartments in PC-$Ca_v2.1$ KO mice at P21. Double immunofluorescence for EAAT4 (***A***$_1$, ***B***$_1$, ***C***$_1$, ***C***$_2$, ***D***$_1$, ***D***$_2$) and aldolase C (aldC; ***A***$_2$, ***B***$_2$, ***C***$_1$, ***C***$_3$, ***D***$_1$, ***D***$_3$) in control mice (***A***, ***C***) and PC-$Ca_v2.1$ KO mice (***B***, ***D***) at P21. In control mice, EAAT4-strong bands closely match with aldolase C(+) bands (double-headed arrows in ***C***$_2$, ***C***$_3$). In PC-$Ca_v2.1$ KO mice, the boundary of EAAT4 compartments is less obvious and EAAT4-dominant bands are wider than aldolase C(+) bands (double-headed arrows in ***D***$_2$, ***D***$_3$). Numerals 3–6 indicate the lobule number. Scale bars: ***A***, 200 μm; ***C***, 100 μm. ***E***, Histograms showing the relative width of the cerebellar band. The values for EAAT4 are 17.8 $\pm$ 1.7% in control and 25.0 $\pm$ 1.6% in PC-$Ca_v2.1$ KO mice, $p < 0.05$, whereas those for aldolase C are 16.5 $\pm$ 2.1% in control and 17.5 $\pm$ 1.3% in PC-$Ca_v2.1$ KO mice, $p = 0.77$ (mean $\pm$ SEM, $n = 3$ mice, *U* test). ***F***, Histograms showing the relative intensity gap. The values for EAAT4 are 163.9 $\pm$ 5.3% in control and 147.1 $\pm$ 5.7% in PC-$Ca_v2.1$ KO mice, $p < 0.05$, whereas those for aldolase C are 255.1 $\pm$ 11.8% in control and 265.5 $\pm$ 10.5% in PC-$Ca_v2.1$ KO mice, $p = 0.28$ (mean $\pm$ SEM, $n = 3$ mice, *U* test). White and black bars indicate control and PC-$Ca_v2.1$ KO mice, respectively. *$p < 0.05$.

terminals contacting with multiple spines, proximal retraction of CF territory, and persistence of multiple CF innervation in almost all PCs (Rhyu et al., 1999a,b; Miyazaki et al., 2004). Of these phenotypes, the severe persistence of multiple CF innervation points to its essential role in homosynaptic competition among CF inputs (Miyazaki et al., 2004). Using PC-$Ca_v2.1$ KO mice, we recently reported that the impaired homosynaptic competition is caused by the lack of postsynaptic $Ca_v2.1$, resulting in equal functional strengthening and dendritic translocation of multiple CF inputs (Hashimoto et al., 2011). Conversely, the shifted innervation territory in global $Ca_v2.1$ KO mice, i.e., expanded PF territory and retracted CF territory, has been interpreted to mean that $Ca_v2.1$ also promotes heterosynaptic competition to the advantage of CFs over PFs (Miyazaki et al., 2004). In the present study, the shifted territory was reproduced in PC-$Ca_v2.1$ KO mice but not in GC-$Ca_v2.1$ KO mice, indicating that postsynaptic $Ca_v2.1$ also consolidates CF innervation at proximal dendrites and expels PF inputs to distal dendrites. Together, these findings indicate that postsynaptic $Ca_v2.1$ regulates excitatory wiring in PCs by giving single winner CFs a competitive advantage over PFs and surplus CFs, thereby enabling it to establish well-organized excitatory wiring in PCs.

In the heterosynaptic competition, global GluRδ2 KO mice exhibit the opposite phenotype, i.e., PF synaptogenesis is impaired at distal dendrites and CF territory expands to distal dendrites (Kashiwabuchi et al., 1995; Kurihara et al., 1997; Ichikawa et al., 2002). This suggests that GluRδ2 endows PFs with a competitive advantage over CFs and that the development of functional PC circuits is based on a competitive equilibrium promoted by $Ca_v2.1$ and GluRδ2. Intriguingly, regressed CF territory and expanded PF territory are also induced in adulthood by silencing afferent activities with tetrodotoxin (Bravin et al., 1999). In addition, perisomatic innervation by CFs revives in adult PCs by mechanical lesions of the cerebellar cortex and genetic defects causing PC degeneration (Rossi et al., 1995).

Furthermore, wiring defects in global GluRδ2 KO mice are reproduced when GluRδ2 is ablated in adult mice (Takeuchi et al., 2005; Miyazaki et al., 2010). These findings indicate that the maintenance of functional PC circuits in adulthood is also based on a competitive equilibrium, which is probably controlled by GluRδ2 and its counter-mechanisms, most likely $Ca_v2.1$. The role of $Ca_v2.1$ in the maintenance of functional circuitry needs to be addressed in future studies by using the conditional $Ca_v2.1$ KO system in adult subjects.

Global $Ca_v2.1$ KO mice further manifest considerable enlargement of PF terminals and their aberrant contact with multiple PC spines (Miyazaki et al., 2004). The presynaptic phenotypes at PF–PC synapses were reproduced in PC-$Ca_v2.1$ KO mice but not in GC-$Ca_v2.1$ KO mice. This finding highlights the fact that $Ca_v2.1$-mediated Ca^{2+} signaling and dynamics in PCs retrogradely affect the size, shape, and contact number of PF terminals. Consistent with these morphological alternations, synaptic transmission at PF–PC synapses is markedly enhanced and, herein, demonstrated an increase in the unitary EPSC amplitude that was presumably attributable to the elevated release probability and increased contact number of individual PF terminals to PC spines. It has been demonstrated that homeostatic increase of presynaptic release function is induced by postsynaptic glutamate receptor blockade (Frank et al., 2006). Therefore, these changes at PF–PC synapses in PC-$Ca_v2.1$ KO mice might result from such synaptic scaling mechanisms to compensate for insufficient postsynaptic Ca^{2+} signaling or/and reduced density of PF–PC synapses.

PCs in aldolase C-negative compartments are more vulnerable to $Ca_v2.1$ deprivation

In PC-$Ca_v2.1$ KO mice, PC degeneration started in the third postnatal week and preferentially occurred in aldolase(−) PC compartments. Such a patterned PC degeneration often occurs in spontaneous and gene-manipulated mutants (Wassef et al., 1987; Sarna and Hawkes, 2003; Dusart et al., 2006). In spontaneous $Ca_v2.1$ mutant mice, such as the so-called *leaner* and *tottering* mice, a patterned PC loss takes place in aldolase C(−) PC compartments (Herrup and Wilczynski, 1982; Heckroth and Abbott, 1994; Sawada et al., 2009). PC degeneration also occurs in human defective the $Ca_v2.1$ gene, such as familial hemiplegic migraine and episodic ataxia type-2 (Elliott et al., 1996; Ophoff et al., 1996; Kors et al., 2001; Mochizuki et al., 2004). In the so-called *nervous* mutant mice, in contrast, patterned PC degeneration occurs in aldolase C(+) PC compartments (Wassef et al., 1987; Dusart et al., 2006). Thus, the survival of PCs is regulated by multiple genes and molecules, of which PCs in aldolase C(−) compartments are more vulnerable than those in aldolase C(+) compartments to the loss of $Ca_v2.1$.

When comparing the onset of degeneration between different mice strains, degeneration starts much earlier in PC-$Ca_v2.1$ KO mice (3 weeks of age) than in the *leaner* (1.5 months) and *tottering* (12 months) mice (Herrup and Wilczynski, 1982; Heckroth and Abbott, 1994; Sawada et al., 2009). Because the slower onset in the *tottering* mice has been attributed to a milder defect in Ca^{2+} influx compared with the *leaner* mice (Lorenzon et al., 1998; Wakamori et al., 1998; Dove et al., 2000), the very early onset in PC-$Ca_v2.1$ KO mice is likely attributable to the complete lack of $Ca_v2.1$-mediated Ca^{2+} influx in PCs (Hashimoto et al., 2011). Conversely, the onset of patterned PC degeneration in global $Ca_v2.1$ KO mice occurs at 15 weeks of age (Fletcher et al., 2001), suggesting that a concomitant defect of presynaptic $Ca_v2.1$ might offset the loss of postsynaptic $Ca_v2.1$ and eventually alleviate PC degeneration.

$Ca_v2.1$ regulates compartmental expression by posttranscriptional modification

We have shown previously that PLCβ3 and PLCβ4 exhibit banded expression across the cerebellum (Kano et al., 1998). The present study further investigated whether some PCs in peri-boundary regions coexpressed PLCβ3 and PLCβ4 mRNAs. The indistinct boundary at the transcription level contrasts with the sharp boundary at the protein level, which is clearly revealed by the non-overlapping immunolabeling of dendritic trees for PLCβ3 and PLCβ4 (Nomura et al., 2007; Fukaya et al., 2008). These findings show that, although the gross framework of compartmental PLCβ3 and PLCβ4 expression is determined at the transcription level, this framework needs posttranscriptional editing to shape it into a more precisely reciprocal framework.

In PC-$Ca_v2.1$ KO mice, expression patterns of PLCβ3 and PLCβ4 mRNAs were similar to those in control mice. By immunohistochemistry, PLCβ4 banding in the molecular layer was also comparable with that in control mice in terms of the onset, width, location, and relative intensity gap between PLCβ3- and PLCβ4-dominant compartments. However, PLCβ3 banding, which normally develops during the second and third postnatal weeks by its downregulation in PLCβ4-dominant compartments, was affected in PC-$Ca_v2.1$ KO mice. Accordingly, some PCs in PLCβ4-dominant compartments retained moderate levels of PLCβ3, leading to a blurred boundary in PC-$Ca_v2.1$ KO mice. Thus, $Ca_v2.1$ in PCs is involved in the posttranscriptional modification of PLCβ3, by which PLCβ3 is downregulated at the protein level in aldolase C(−) compartments and acquires precise reciprocity to the preexisting banding of PLCβ4. In addition, we found increased perikaryal accumulation of PLCβ3 and PLCβ4 in PC-$Ca_v2.1$ KO mice. Based on these findings, it is conceivable that $Ca_v2.1$-mediated posttranscriptional modification may affect protein synthesis, trafficking, and/or degradation of PLCβs in a compartment-specific manner.

Hsp25, HNK1 antigen, EAAT4, and protein kinase C-δ are compartment markers and expressed predominantly in aldolase C(+) compartments (Chen and Hillman, 1993; Eisenman and Hawkes, 1993; Nagao et al., 1997; Dehnes et al., 1998; Armstrong and Hawkes, 2000; Barmack et al., 2000). Of these, we further investigated the altered boundaries in EAAT4 compartments. Like PLCβ3, the border of EAAT4-strong and EAAT4-weak bands was obscured and mismatched with that of aldolase C compartments in PC-$Ca_v2.1$ KO mice. Thus, $Ca_v2.1$ appears to sculpt the boundary of some, if not all, of the cerebellar compartment markers.

In conclusion, $Ca_v2.1$ expressed in PCs regulates competitive excitatory wiring, cell survival, and the precise reciprocity and boundary of cerebellar biochemical compartments by PLCβ3 and EAAT4.

References

Abe M, Fukaya M, Yagi T, Mishina M, Watanabe M, Sakimura K (2004) NMDA receptor GluRe/NR2 subunits are essential for postsynaptic localization and protein stability of GluRz1/NR1 subunit. J Neurosci 24:7292–7304.

Altman J (1972) Postnatal development of the cerebellar cortex in the rat. II. Phases in the maturation of Purkinje cells and of the molecular layer. J Comp Neurol 145:399–463.

Araki K, Araki M, Miyazaki J, Vassalli P (1995) Site-specific recombination of a transgene in fertilized eggs by transient expression of Cre recombinase. Proc Natl Acad Sci U S A 92:160–164.

Armstrong CL, Hawkes R (2000) Pattern formation in the cerebellar cortex. Biochem Cell Biol 78:551–562.

Barmack NH, Qian Z, Yoshimura J (2000) Regional and cellular distribution of protein kinase C in rat cerebellar Purkinje cells. J Comp Neurol 427:235–254.

Bekkers JM, Clements JD (1999) Quantal amplitude and quantal variance of strontium-induced asynchronous EPSCs in rat dentate granule neurons. J Physiol 516:227–248.

Bravin M, Rossi F, Strata P (1995) Different climbing fibres innervate separate dendritic regions of the same Purkinje cell in hypogranular cerebellum. J Comp Neurol 357:395–407.

Bravin M, Morando L, Vercelli A, Rossi F, Strata P (1999) Control of spine formation by electrical activity in the adult rat cerebellum. Proc Natl Acad Sci U S A 96:1704–1709.

Chedotal A, Sotelo C (1992) Early development of olivocerebellar projections in the fetal rat using CGRP immunocytochemistry. Eur J Neurosci 4:1159–1179.

Chedotal A, Sotelo C (1993) The "creeper stage" in cerebellar climbing fiber synaptogenesis precedes the "pericellular nest"—ultrastructural evidence with parvalbumin immunocytochemistry. Brain Res Dev Brain Res 76:207–220.

Chen S, Hillman DE (1993) Compartmentation of the cerebellar cortex by protein kinase C delta. Neuroscience 56:177–188.

Crepel F, Delhaye-Bouchaud N, Dupont JL (1981) Fate of the multiple innervation of cerebellar Purkinje cells by climbing fibers in immature control, x-irradiated and hypothyroid rats. Brain Res 227:59–71.

Dehnes Y, Chaudhry FA, Ullensvang K, Lehre KP, Storm-Mathisen J, Danbolt NC (1998) The glutamate transporter EAAT4 in rat cerebellar Purkinje cells: a glutamate-gated chloride channel concentrated near the synapse in parts of the dendritic membrane facing astroglia. J Neurosci 18:3606–3619.

Dove LS, Nahm SS, Murchison D, Abbott LC, Griffith WH (2000) Altered calcium homeostasis in cerebellar Purkinje cells of leaner mutant mice. J Neurophysiol 84:513–524.

Dusart I, Guenet JL, Sotelo C (2006) Purkinje cell death: differences between developmental cell death and neurodegenerative death in mutant mice. Cerebellum 5:163–173.

Eisenman LM, Hawkes R (1993) Antigenic compartmentation in the mouse cerebellar cortex: zebrin and HNK-1 reveal a complex, overlapping molecular topography. J Comp Neurol 335:586–605.

Elliott MA, Peroutka SJ, Welch S, May EF (1996) Familial hemiplegic migraine, nystagmus, and cerebellar atrophy. Ann Neurol 39:100–106.

Fletcher CF, Tottene A, Lennon VA, Wilson SM, Dubel SJ, Paylor R, Hosford DA, Tessarollo L, McEnery MW, Pietrobon D, Copeland NG, Jenkins NA (2001) Dystonia and cerebellar atrophy in *Cacna1a* null mice lacking P/Q calcium channel activity. FASEB J 15:1288–1290.

Frank CA, Kennedy MJ, Goold CP, Marek KW, Davis GW (2006) Mechanisms underlying the rapid induction and sustained expression of synaptic homeostasis. Neuron 52:663–677.

Fremeau RT Jr, Troyer MD, Pahner I, Nygaard GO, Tran CH, Reimer RJ, Bellocchio EE, Fortin D, Storm-Mathisen J, Edwards RH (2001) The expression of vesicular glutamate transporters defines two classes of excitatory synapse. Neuron 31:247–260.

Fukaya M, Tsujita M, Yamazaki M, Kushiya E, Abe M, Akashi K, Natsume R, Kano M, Kamiya H, Watanabe M, Sakimura K (2006) Abundant distribution of TARP g-8 in synaptic and extrasynaptic surface of hippocampal neurons and its major role in AMPA receptor expression on spines and dendrites. Eur J Neurosci 24:2177–2190.

Fukaya M, Uchigashima M, Nomura S, Hasegawa Y, Kikuchi H, Watanabe M (2008) Predominant expression of phospholipase Cb1 in telencephalic principal neurons and cerebellar interneurons, and its close association with related signaling molecules in somatodendritic neuronal elements. Eur J Neurosci 28:1744–1759.

Fuse T, Kanai Y, Kanai-Azuma M, Suzuki M, Nakamura K, Mori H, Hayashi Y, Mishina M (2004) Conditional activation of RhoA suppresses the epithelial to mesenchymal transition at the primitive streak during mouse gastrulation. Biochem Biophys Res Commun 318:665–672.

Hashimoto K, Kano M (2003) Functional differentiation of multiple climbing fiber inputs during synapse elimination in the developing cerebellum. Neuron 38:785–796.

Hashimoto K, Ichikawa R, Kitamura K, Watanabe M, Kano M (2009) Translocation of a "winner" climbing fiber to the Purkinje cell dendrite and subsequent elimination of "losers" from the soma in developing cerebellum. Neuron 63:106–118.

Hashimoto K, Tsujita M, Miyazaki T, Kitamura K, Yamazaki M, Shin HS, Watanabe M, Sakimura K, Kano M (2011) Postsynaptic P/Q-type Ca^{2+} channel in Purkinje cell mediates synaptic competition and elimination in developing cerebellum. Proc Natl Acad Sci U S A 108:9987–9992.

Hawkes R (1997) An anatomical model of cerebellar modules. Prog Brain Res 114:39–52.

Hawkes R, Eisenman LM (1997) Stripes and zones: the origins of regionalization of the adult cerebellum. Perspect Dev Neurobiol 5:95–105.

Heckroth JA, Abbott LC (1994) Purkinje cell loss from alternating sagittal zones in the cerebellum of leaner mutant mice. Brain Res 658:93–104.

Herrup K, Kuemerle B (1997) The compartmentalization of the cerebellum. Annu Rev Neurosci 20:61–90.

Herrup K, Wilczynski SL (1982) Cerebellar cell degeneration in the leaner mutant mouse. Neuroscience 7:2185–2196.

Hirai H, Pang Z, Bao D, Miyazaki T, Li L, Miura E, Parris J, Rong Y, Watanabe M, Yuzaki M, Morgan JI (2005) Cbln1 is essential for synaptic integrity and plasticity in the cerebellum. Nat Neurosci 8:1534–1541.

Ichikawa R, Miyazaki T, Kano M, Hashikawa T, Tatsumi H, Sakimura K, Mishina M, Inoue Y, Watanabe M (2002) Distal extension of climbing fiber territory and multiple innervation caused by aberrant wiring to adjacent spiny branchlets in cerebellar Purkinje cells lacking glutamate receptor d2. J Neurosci 22:8487–8503.

Ichikawa R, Yamasaki M, Miyazaki T, Konno K, Hashimoto K, Tatsumi H, Inoue Y, Kano M, Watanabe M (2011) Developmental switching of perisomatic innervation from climbing fibers to basket cell fibers in cerebellar Purkinje cells. J Neurosci 31:16916–16927.

Kano M, Rexhausen U, Dreessen J, Konnerth A (1992) Synaptic excitation produces a long-lasting rebound potentiation of inhibitory synaptic signals in cerebellar Purkinje cells. Nature 356:601–604.

Kano M, Hashimoto K, Chen C, Abeliovich A, Aiba A, Kurihara H, Watanabe M, Inoue Y, Tonegawa S (1995) Impaired synapse elimination during cerebellar development in PKCg mutant mice. Cell 83:1223–1231.

Kano M, Hashimoto K, Kurihara H, Watanabe M, Inoue Y, Aiba A, Tonegawa S (1997) Persistent multiple climbing fiber innervation of cerebellar Purkinje cells in mice lacking mGluR1. Neuron 18:71–79.

Kano M, Hashimoto K, Watanabe M, Kurihara H, Offermanns S, Jiang H, Wu Y, Jun K, Shin HS, Inoue Y, Simon MI, Wu D (1998) Phospholipase Cb4 is specifically involved in climbing fiber synapse elimination in the developing cerebellum. Proc Natl Acad Sci U S A 95:15724–15729.

Kashiwabuchi N, Ikeda K, Araki K, Hirano T, Shibuki K, Takayama C, Inoue Y, Kutsuwada T, Yagi T, Kang Y, Aizawa S, Mishina M (1995) Impairment of motor coordination, Purkinje cell synapse formation, and cerebellar long-term depression in GluR d2 mutant mice. Cell 81:245–252.

Konnerth A, Llano I, Armstrong CM (1990) Synaptic currents in cerebellar Purkinje cells. Proc Natl Acad Sci U S A 87:2662–2665.

Konnerth A, Dreessen J, Augustine GJ (1992) Brief dendritic calcium signals initiate long-lasting synaptic depression in cerebellar Purkinje cells. Proc Natl Acad Sci U S A 89:7051–7055.

Kors EE, Terwindt GM, Vermeulen FL, Fitzsimons RB, Jardine PE, Heywood P, Love S, van den Maagdenberg AM, Haan J, Frants RR, Ferrari MD (2001) Delayed cerebral edema and fatal coma after minor head trauma: role of the CACNA1A calcium channel subunit gene and relationship with familial hemiplegic migraine. Ann Neurol 49:753–760.

Kurihara H, Hashimoto K, Kano M, Takayama C, Sakimura K, Mishina M, Inoue Y, Watanabe M (1997) Impaired parallel fiber→Purkinje cell synapse stabilization during cerebellar development of mutant mice lacking the glutamate receptor d2 subunit. J Neurosci 17:9613–9623.

Larouche M, Hawkes R (2006) From clusters to stripes: the developmental origins of adult cerebellar compartmentation. Cerebellum 5:77–88.

Larramendi LMH (1969) Analysis of synaptogenesis in the cerebellum of the mouse. In: Neurobiology of cerebellar evolution and development (Llinàs R, ed), pp 803–843. Chicago: American Medical Association/Education and Research Foundation.

Lorenzon NM, Lutz CM, Frankel WN, Beam KG (1998) Altered calcium channel currents in Purkinje cells of the neurological mutant mouse *leaner*. J Neurosci 18:4482–4489.

Mariani J (1982) Extent of multiple innervation of Purkinje cells by climbing fibers in the olivocerebellar system of weaver, reeler, and staggerer mutant mice. J Neurobiol 13:119–126.

Mark MD, Maejima T, Kuckelsberg D, Yoo JW, Hyde RA, Shah V, Gutierrez D, Moreno RL, Kruse W, Noebels JL, Herlitze S (2011) Delayed postnatal loss of P/Q-type calcium channels recapitulates the absence epilepsy, dyskinesia, and ataxia phenotypes of genomic *Cacna1A* mutations. J Neurosci 31:4311–4326.

Marzban H, Chung S, Watanabe M, Hawkes R (2007) Phospholipase cb4

expression reveals the continuity of cerebellar topography through development. J Comp Neurol 502:857–871.
Mintz IM, Venema VJ, Swiderek KM, Lee TD, Bean BP, Adams ME (1992) P-type calcium channels blocked by the spider toxin w-Aga-IVA. Nature 355:827–829.
Mintz IM, Sabatini BL, Regehr WG (1995) Calcium control of transmitter release at a cerebellar synapse. Neuron 15:675–688.
Mishina M, Sakimura K (2007) Conditional gene targeting on the pure C57BL/6 genetic background. Neurosci Res 58:105–112.
Mitani A, Watanabe M, Kataoka K (1998) Functional change of NMDA receptors related to enhancement of susceptibility to neurotoxicity in the developing pontine nucleus. J Neurosci 18:7941–7952.
Miyazaki T, Watanabe M (2011) Development of an anatomical technique for visualizing the mode of climbing fiber innervation in Purkinje cells and its application to mutant mice lacking GluRd2 and $Ca_V2.1$. Anat Sci Int 86:10–18.
Miyazaki T, Fukaya M, Shimizu H, Watanabe M (2003) Subtype switching of vesicular glutamate transporters at parallel fibre–Purkinje cell synapses in developing mouse cerebellum. Eur J Neurosci 17:2563–2572.
Miyazaki T, Hashimoto K, Shin HS, Kano M, Watanabe M (2004) P/Q-type Ca^{2+} channel a1A regulates synaptic competition on developing cerebellar Purkinje cells. J Neurosci 24:1734–1743.
Miyazaki T, Yamasaki M, Takeuchi T, Sakimura K, Mishina M, Watanabe M (2010) Ablation of glutamate receptor GluRd2 in adult Purkinje cells causes multiple innervation of climbing fibers by inducing aberrant invasion to parallel fiber innervation territory. J Neurosci 30:15196–15209.
Mochizuki Y, Kawata A, Mizutani T, Takamoto K, Hayashi H, Taki K, Morimatsu Y (2004) Hereditary paroxysmal ataxia with mental retardation: a clinicopathological study in relation to episodic ataxia type 2. Acta Neuropathol 108:345–349.
Morara S, van der Want JJ, de Weerd H, Provini L, Rosina A (2001) Ultrastructural analysis of climbing fiber–Purkinje cell synaptogenesis in the rat cerebellum. Neuroscience 108:655–671.
Nagao S, Kwak S, Kanazawa I (1997) EAAT4, a glutamate transporter with properties of a chloride channel, is predominantly localized in Purkinje cell dendrites, and forms parasagittal compartments in rat cerebellum. Neuroscience 78:929–933.
Nakagawa S, Watanabe M, Isobe T, Kondo H, Inoue Y (1998) Cytological compartmentalization in the staggerer cerebellum, as revealed by calbindin immunohistochemistry for Purkinje cells. J Comp Neurol 395:112–120.
Nakamura K, Manabe T, Watanabe M, Mamiya T, Ichikawa R, Kiyama Y, Sanbo M, Yagi T, Inoue Y, Nabeshima T, Mori H, Mishina M (2001) Enhancement of hippocampal LTP, reference memory and sensorimotor gating in mutant mice lacking a telencephalon-specific cell adhesion molecule. Eur J Neurosci 13:179–189.
Nakamura M, Sato K, Fukaya M, Araishi K, Aiba A, Kano M, Watanabe M (2004) Signaling complex formation of phospholipase Cb4 with metabotropic glutamate receptor type 1a and 1,4,5-trisphosphate receptor at the perisynapse and endoplasmic reticulum in the mouse brain. Eur J Neurosci 20:2929–2944.
Nomura S, Fukaya M, Tsujioka T, Wu D, Watanabe M (2007) Phospholipase Cb3 is distributed in both somatodendritic and axonal compartments and localized around perisynapse and smooth endoplasmic reticulum in mouse Purkinje cell subsets. Eur J Neurosci 25:659–672.
Offermanns S, Hashimoto K, Watanabe M, Sun W, Kurihara H, Thompson RF, Inoue Y, Kano M, Simon MI (1997) Impaired motor coordination and persistent multiple climbing fiber innervation of cerebellar Purkinje cells in mice lacking Gaq. Proc Natl Acad Sci U S A 94:14089–14094.
Ophoff RA, Terwindt GM, Vergouwe MN, van Eijk R, Oefner PJ, Hoffman SM, Lamerdin JE, Mohrenweiser HW, Bulman DE, Ferrari M, Haan J, Lindhout D, van Ommen GJ, Hofker MH, Ferrari MD, Frants RR (1996) Familial hemiplegic migraine and episodic ataxia type-2 are caused by mutations in the Ca^{2+} channel gene CACNL1A4. Cell 87:543–552.
Palay S, Chan-Palay V (1974) Cerebellar cortex: cytology and organization, pp 63–69, 242–287. New York: Springer.
Ramón y Cajal S (1911) Histologie du Système Nerveux de l'Homme et des Vertébrés, Vol II. Paris: Maloine.
Regehr WG, Mintz IM (1994) Participation of multiple calcium channel types in transmission at single climbing fiber to Purkinje cell synapses. Neuron 12:605–613.
Rhyu IJ, Abbott LC, Walker DB, Sotelo C (1999a) An ultrastructural study of granule cell/Purkinje cell synapses in tottering (*tg/tg*), leaner (tg^{la}/tg^{la}) and compound heterozygous tottering/leaner (tg/tg^{la}) mice. Neuroscience 90:717–728.
Rhyu IJ, Oda S, Uhm CS, Kim H, Suh YS, Abbott LC (1999b) Morphologic investigation of rolling mouse Nagoya (tg^{rol}/tg^{rol}) cerebellar Purkinje cells: an ataxic mutant, revisited. Neurosci Lett 266:49–52.
Rossi F, Jankovski A, Sotelo C (1995) Target neuron controls the integrity of afferent axon phenotype: a study on the Purkinje cell-climbing fiber system in cerebellar mutant mice. J Neurosci 15:2040–2056.
Sarna JR, Hawkes R (2003) Patterned Purkinje cell death in the cerebellum. Prog Neurobiol 70:473–507.
Sarna JR, Marzban H, Watanabe M, Hawkes R (2006) Complementary stripes of phospholipase Cb3 and Cb4 expression by Purkinje cell subsets in the mouse cerebellum. J Comp Neurol 496:303–313.
Sawada K, Kalam Azad A, Sakata-Haga H, Lee NS, Jeong YG, Fukui Y (2009) Striking pattern of Purkinje cell loss in cerebellum of an ataxic mutant mouse, *tottering.* Acta Neurobiol Exp (Wars) 69:138–145.
Stea A, Tomlinson WJ, Soong TW, Bourinet E, Dubel SJ, Vincent SR, Snutch TP (1994) Localization and functional properties of a rat brain a_{1A} calcium channel reflect similarities to neuronal Q- and P-type channels. Proc Natl Acad Sci U S A 91:10576–10580.
Sugihara I, Wu H, Shinoda Y (1999) Morphology of single olivocerebellar axons labeled with biotinylated dextran amine in the rat. J Comp Neurol 414:131–148.
Sugihara I, Bailly Y, Mariani J (2000) Olivocerebellar climbing fibers in the granuloprival cerebellum: morphological study of individual axonal projections in the X-irradiated rat. J Neurosci 20:3745–3760.
Takeuchi T, Miyazaki T, Watanabe M, Mori H, Sakimura K, Mishina M (2005) Control of synaptic connection by glutamate receptor d2 in the adult cerebellum. J Neurosci 25:2146–2156.
Todorov B, Kros L, Shyti R, Plak P, Haasdijk ED, Raike RS, Frants RR, Hess EJ, Hoebeek FE, De Zeeuw CI, van den Maagdenberg AM (2011) Purkinje cell-specific ablation of $Ca_V2.1$ channels is sufficient to cause cerebellar ataxia in mice. Cerebellum. Advance online publication. Retrieved December 12, 2011. doi:10.1007/s12311-011-0302-1.
Tsujita M, Mori H, Watanabe M, Suzuki M, Miyazaki J, Mishina M (1999) Cerebellar granule cell-specific and inducible expression of Cre recombinase in the mouse. J Neurosci 19:10318–10323.
Wakamori M, Yamazaki K, Matsunodaira H, Teramoto T, Tanaka I, Niidome T, Sawada K, Nishizawa Y, Sekiguchi N, Mori E, Mori Y, Imoto K (1998) Single tottering mutations responsible for the neuropathic phenotype of the P-type calcium channel. J Biol Chem 273:34857–34867.
Wassef M, Sotelo C, Cholley B, Brehier A, Thomasset M (1987) Cerebellar mutations affecting the postnatal survival of Purkinje cells in the mouse disclose a longitudinal pattern of differentially sensitive cells. Dev Biol 124:379–389.
Watanabe M, Kano M (2011) Climbing fiber synapse elimination in cerebellar Purkinje cells. Eur J Neurosci 34:1697–1710.
Watanabe M, Inoue Y, Sakimura K, Mishina M (1992) Developmental changes in distribution of NMDA receptor channel subunit mRNAs. Neuroreport 3:1138–1140.
Westenbroek RE, Sakurai T, Elliott EM, Hell JW, Starr TV, Snutch TP, Catterall WA (1995) Immunochemical identification and subcellular distribution of the a_{1A} subunits of brain calcium channels. J Neurosci 15:6403–6418.
Woodward DJ, Hoffer BJ, Altman J (1974) Physiological and pharmacological properties of Purkinje cells in rat cerebellum degranulated by postnatal x-irradiation. J Neurobiol 5:283–304.
Yamada K, Watanabe M, Shibata T, Tanaka K, Wada K, Inoue Y (1996) EAAT4 is a post-synaptic glutamate transporter at Purkinje cell synapses. Neuroreport 7:2013–2017.
Yamasaki M, Yamada K, Furuya S, Mitoma J, Hirabayashi Y, Watanabe M (2001) 3-Phosphoglycerate dehydrogenase, a key enzyme for L-serine biosynthesis, is preferentially expressed in the radial glia/astrocyte lineage and olfactory ensheathing glia in the mouse brain. J Neurosci 21:7691–7704.
Yamasaki M, Matsui M, Watanabe M (2010) Preferential localization of muscarinic M1 receptor on dendritic shaft and spine of cortical pyramidal cells and its anatomical evidence for volume transmission. J Neurosci 30:4408–4418.
Yanagawa Y, Kobayashi T, Ohnishi M, Kobayashi T, Tamura S, Tsuzuki T, Sanbo M, Yagi T, Tashiro F, Miyazaki J (1999) Enrichment and efficient screening of ES cells containing a targeted mutation: the use of DT-A gene with the polyadenylation signal as a negative selection maker. Transgenic Res 8:215–221.